Reconstructing the effects of hurricanes over 155 years on the structure and diversity of trees in two tropical montane rainforests in Jamaica

McLaren, Kurt; Luke, Denneko; Tanner, Edmund ; Bellingham, Peter J; Healey, John

Agricultural and Forest Meteorology

DOI:
10.1016/j.agrformet.2019.107621

Published: 15/10/2019

Peer reviewed version

Reconstructing the effects of hurricanes over 155 years on the structure and diversity of trees in two tropical montane rain forests in Jamaica

Kurt McLaren[a*] , Denneko Luke[a], Edmund Tanner[b], Peter J Bellingham[c] and John R Healey[d]

[a]Department of Life Sciences, University of the West Indies, Mona, Kingston 7, Jamaica

[b] Department of Plant Sciences, University of Cambridge, Downing Street, Cambridge CB2 3EA, United Kingdom.

[c] Manaaki Whenua – Landcare Research, P. O. Box 69040, Lincoln 7640, New Zealand

[d]School of Natural Sciences, Bangor University, Bangor, Gwynedd, LL57 2UW, United Kingdom

* Corresponding author: Tel: +18769272753; Email address: kurt.mclaren@uwimona.edu.jm

Abstract

The effects of the spatiotemporal (> 100 years) range of hurricane disturbance intensity on tree diversity and density patterns are largely unknown, because data on past stand or landscape scale hurricane impacts are sometimes unavailable. We therefore reconstructed and mapped topographic exposure (a proxy to disturbance) to twelve category 2–4 hurricanes that affected the rain forests of the Blue Mountains (BM) and the John Crow Mountains (JCM) in Jamaica, over 155 years. Maps of average topographic exposure and the spatial outputs from a pixel-based polynomial regression of the cardinal directions of the tracks of past hurricanes (predictor) and past exposure (response) were then used to represent the aggregate spatiotemporal range of exposure. Next, we used data collected over the period 1974-2009 from 35, 10 x10 m nested subplots and 1991-2004 from 16, 200 m^2 circular plots for the BM and 2006-2012 from 45, 25 x 25 m plots for the JCM, and Bayesian spatiotemporal, Integrated Nested Laplace Approximation (INLA) models to determine whether stand-level (≈ 1 km^2) tree Shannon diversity and density patterns were primarily influenced by exposure to a single hurricane, the most severe hurricane or to multiple hurricanes and the duration of hurricane effects on Shannon diversity and tree density. In the BM, long-term diversity peaked at locations with intermediate values of average exposure for six hurricanes (five of which made landfall over the period 1903-1988). Short-term diversity peaked at locations that experienced significantly higher exposure situated to the south or north of the hurricane's track when the tracks were to the north or south of the island, respectively. Short-term density peaked at locations that were always highly exposed. Moreover, the influence of the most severe hurricane on diversity can last up to 101 years and the influence of the most recent hurricane (Gilbert) on diversity became evident after 16 - 21 years. The JCM was more susceptible to hurricanes and this diminished the influence of past hurricanes.

Consequently, density peaked at sites with the highest average exposure to the four most recent hurricanes (1988-2007), only one of which made landfall. If historical hurricane disturbance data are unavailable, reconstructed exposure maps can be used to provide valuable insights into the effects of past hurricanes on stand-level tree diversity and density patterns.

Keywords: Bayesian; Integrated Nested Laplace Approximation; intermediate disturbance hypothesis; topographic exposure; spatiotemporal models; cyclone; forest structure.

Introduction

Tropical forests on most islands worldwide are subject to repeated effects of tropical cyclones (also referred to regionally as hurricanes and typhoons) (Boose et al. 2004; Bellingham 2008). As a hurricane moves across a forested landscape, meteorological, biological and topographic factors interact to create complex patterns of damage at different spatial scales (Xi et al. 2008). At the ecosystem level (e.g. forest stands), hurricanes cause leaf stripping, branch breakage or loss, snapping of tree crowns and uprooting, and individual and multi-tree blow downs (Boose et al. 1994; Boose et al. 2004; Rossi et al. 2017). At landscape scales, hurricane impacts are generally heterogeneous and, as such, there are usually gradients of damage and mortality across the landscape (Gannon and Martin 2014). The heterogeneity of forest damage is determined by wind velocity gradients that result from the intensity, size and proximity of a hurricane, and their interaction with the abiotic and biotic attributes of a landscape (Zimmerman et al. 1994; Everham and Brokaw 1996; Boose et al. 2004). The abiotic attributes of a landscape that contribute to the heterogeneity of forest disturbance include soils and geomorphology, both of

which affect windthrow vulnerability and landslide distribution and local topography which determines differences in site exposure (Bellingham, 1991; Scatena and Larsen, 1991; Zimmerman et al. 1994; Everham and Brokaw 1996; Boose et al. 1994; Gannon and Martin 2014). Biotic features such as forest type, species composition, structural attributes and the characteristics of tree species (stem size [height and diameter], architecture and wood density as examples) influence the susceptibility and response of trees and forest stands to wind damage, and contribute to the heterogeneity of forest disturbance (Boose et al. 1994; Zimmerman et al. 1994; Everham and Brokaw 1996; Tanner and Bellingham 2006; McGroddy et al. 2013; Gannon and Martin 2014).

The degree of structural change, species composition, and the method and rates of recovery within forested stands across landscapes are affected by the spatial patterns of hurricane disturbance (Runkle, 1985). Recovery of the forest canopy following a hurricane is quite rapid (< 10 years) and normally occurs through tree releafing, sprouting, or recruitment of fast-growing species (Boose et al. 2004). However, depending on the severity of hurricane disturbance, there may be major structural changes, such as a significant reduction in biomass (Weaver 2002; Heartsill Scalley 2017), wood volume, basal area, and canopy height (Luke et al. 2016a; Heartsill Scalley 2017), which may take much longer to recover (> 10 years) (Weaver 2002; Heartsill Scalley 2017). Additionally, over the long-term, trees may experience sudden or delayed mortality and variation in growth rates related to the severity of hurricane damage, alterations in regeneration pathways and successional trajectories, and increased species turnover (Weaver 2002; Boose et al. 2004; Tanner et al. 2014). Moreover, the heterogeneity of disturbance affects spatiotemporal variability in environmental conditions and resources (Roxburgh et al. 2004).

93 This facilitates the recruitment and establishment of species with diverse life history strategies in
94 the community (Tanner and Bellingham 2006; Luke et al. 2016a). Over time, these effects can
95 result in an increase in tree diversity and richness in forests (Denslow 1995; Vandermeer et al.
96 2000; Tanner and Bellingham 2006; Luke et al. 2016a; Heartsill Scalley 2017) and contribute
97 significantly to tree species coexistence and the maintenance of forest diversity (*sensu*: the
98 intermediate disturbance hypothesis [Connell 1978; Sheil 1999; Shea et al. 2004; Sheil and
99 Burslem 2013]). In addition, there is an increase in stem density in disturbed areas following a
100 hurricane (Tanner and Bellingham 2006) as a lower density of large trees is replaced by more
101 small trees (Denslow 1995). This effect on stem density lasts for many years, even after the
102 canopy has closed (Denslow 1995; Tanner and Bellingham 2006).
103
104 Forest susceptibility to wind damage is also influenced by previous hurricanes, as the impact of a
105 single hurricane event is not independent of past hurricanes (Webb 1958; Boose et al. 2004;
106 Hogan et al. 2018; Ibanez et al. 2019). A total of 152 hurricanes struck the islands of the Greater
107 Antilles, located in the northern Caribbean, between 1851 and 2009 (Gannon and Martin 2014).
108 The hurricane return interval for affected forest sites in the region is on average10 years,
109 although the most that any one site (the far west of Cuba) was struck was 34 times (with a 4.6
110 year hurricane return interval) (Gannon and Martin 2014). As such, trees that live for over 100
111 years in these forests are likely to be affected by many hurricanes during their lifespan (Weaver
112 1986). Therefore, the long-term impact of hurricanes on forest stands can only be understood on
113 a scale of decades to centuries (Boose et al. 1994). Yet, our understanding of hurricane damage,
114 and the mechanisms of short- and long-term recovery at forest sites in the Caribbean, is largely
115 based on stand-level assessments, conducted before and/or after a single hurricane event in

decadal timescales. Meteorological models using data such as historical hurricane track, size, wind speed and wind direction have been used to reconstruct the spatial patterns of disturbance, over different periods (3–158 years) and at various scales (landscape and regional) (e.g. Boose et al. 1994, 2004; Gannon and Martin 2014; Batke et al. 2014; Luke et al. 2016a). However, these data are unavailable for most sites or they have been largely used to explain stand- or landscape-level disturbance patterns and are not often used to explain stand-level fluctuations in tree diversity and density. As a result, the cumulative effects of long-term (> 100 year) hurricane disturbance intensity on forest community responses, such as dynamics and diversity patterns, is less understood. Moreover, the number of high intensity cyhclones is predicted to increase due to the effects of global climate change (Elsner et al. 2008; Bender et al. 2010; Knutson et al. 2010). As a result, forest stands across the Caribbean and in other regions are beginning to become increasingly affected by multiple high-intensity hurricanes (Luke et al. 2016a; Lin et al. 2017, Uriarte et al. 2019). These hurricanes could accelerate structural and compositional changes, particularly at sites that are more exposed to recent and previous hurricane events (Luke et al. 2016a). There is a need to increase our understanding of the impacts of the historical and contemporary range of hurricane disturbance intensity, over space and time, on community dynamics and diversity patterns (Boose et al. 1994; Gannon and Martin 2014; Batke et al. 2014).

Elucidating the effects of past hurricanes on forest stands will require an integrative approach that combines stand-level (≈ 1 km^2) observations with past landscape level (≈ 10 km^2) hurricane disturbance intensity data (e.g. Xi et al. 2008; Luke et al. 2016a). However, there is usually little or no data available on past stand or landscape scale hurricane impacts. It is now possible to generate historical and contemporary landscape scale data on hurricane impacts, due to an

139 increase in the processing power of personal computers and the advent and availability of
140 Geographic Information System (GIS) software, spatial and geographic data and detailed
141 weather data. In addition, the emergence of the interdisciplinary field of geomorphometry, which
142 is concerned with the extraction or quantification of topographic parameters from digital
143 elevation models (DEMs: a digital representation of the terrain or land surface) in a GIS software
144 environment, has been instrumental (Pike et al. 2008; Batke et al. 2014). Topographic exposure
145 is a geomorphometric feature that characterises a site based on the degree of protection it
146 receives from the surrounding landscape and it is the main landscape feature that has been
147 quantified, mapped and used as a proxy for past wind or hurricane disturbance intensity (Ruel et
148 al. 2002; Mikita and Klimánek 2010; Batke et al. 2014; Luke et al. 2016a). Topographic
149 exposure maps have been generated for single and multiple hurricanes (Boose et al. 1994, 2004;
150 Luke et al. 2016a), and average exposure has been calculated based on multiple wind directions
151 (Mikita and Klimánek 2010) and wind inflection angles (Batke et al. 2014), which are used to
152 estimate the wind shadow (Boose et al. 1994). They have also been used to reconstruct > 100
153 years of hurricane disturbance regimes (Boose et al. 1994, 2004). Additionally, data from
154 exposure maps have been extracted and used to determine the cumulative effects of disturbances
155 from three hurricanes on structural changes and diversity at the stand-level (Luke et al. 2016a).
156 However, reconstructed hurricane exposure maps representing > 100 years of hurricane
157 disturbance have never previously been used to determine the cumulative effects of the
158 spatiotemporal range of hurricane disturbances on forest structure and diversity at the stand-
159 level.
160

161 In this study, we therefore sought to determine the cumulated effects of the spatiotemporal (>
162 100 years) range of hurricane disturbances on stand-level spatiotemporal patterns of tree
163 diversity and density. To enable this, we reconstructed topographic exposure maps of hurricanes
164 that affected two adjacent montane sites with a similar disturbance history, the Blue Mountains
165 (BM) and the John Crow Mountains (JCM), in Jamaica, over 155 years (1852–2007). Two
166 methods of aggregating or summarizing the spatiotemporal range or pattern of past hurricane
167 exposure at the landscape scale (≈ 10 km^2) were then evaluated. Luke et al. (2016a) summarized
168 the spatiotemporal range of exposure in the JCM by averaging exposure values extracted from
169 exposure maps for three hurricanes. However, the spatial pattern of exposure or disturbance is
170 also influenced by the distance and the angle/ cardinal direction of the hurricane's eye from and
171 relative to an island or other landmass (Luke et al. 2016a; Boose et al. 1994, 2004). Therefore,
172 we aggregated the spatial and temporal ranges of hurricane exposure by averaging the exposure
173 maps and by modelling the relationship between exposure and the distance or cardinal direction
174 of the tracks of the eye of each hurricanes from or relative to the study sites, and representing
175 these relationships spatially. Data from these maps were then extracted and used to determine
176 whether stand-level (≈ 1 km^2) tree diversity and density spatiotemporal patterns over the periods
177 1974–2009 and 1990–2004 for the BM and 2006–2012 for the JCM, were primarily influenced
178 by exposure to a single hurricane, the most severe hurricane or multiple hurricanes and the
179 duration of hurricane effects on tree diversity and density patterns. We hypothesized that past
180 hurricanes will influence current patterns of diversity by maintaining the highest levels of tree
181 diversity at sites that historically experienced intermediate levels of disturbance. Species
182 coexistence and/or diversity are expected to peak under intermediate disturbance regimes
183 because longer-lived species will not persist if there is too much disturbance and pioneers will be

184 competitively excluded if there is too little disturbance (Connell 1978; Sheil 1999; Shea et al.
185 2004; Sheil and Burslem 2013). We also hypothesized that tree density will be highest at sites
186 that historically experienced the highest levels of disturbance or exposure to hurricanes, on the
187 basis that stands which are frequently exposed to hurricane winds will have continually high
188 turnover rates and hence higher stem densities (Denslow 1995).
189
190 **Study sites**
191 The study sites are forests located on two mountain ranges in Jamaica, the Blue Mountains (BM)
192 and John Crow Mountains (JCM)). Together these ranges comprise the Blue and John Crow
193 Mountains National Park (Figure 1). Data used in this study were measured in plots that were
194 established close to the Grand Ridge of the BM (18° 05′ - 18° 059′ N, 76° 38′ - 76° 40′W) at an
195 elevation of 1320–1920 m in an upper montane tropical forest (Tanner 1977; Tanner and
196 Bellingham, 2006). The data from the JCM were measured in plots established along an
197 altitudinal gradient (400–800 m) at two different sites (18° 3′ N, 76° 21′ 39.6′′ W) (Figure 1).
198 The JCM have a maximum elevation of 1143 m asl and the plots were established in both lower
199 and upper montane tropical forests (Luke et al. 2016a). Both sites have been affected by
200 hurricanes and the resulting effects on the forests have been documented: Hurricane Gilbert
201 (1988) (Bellingham 1991; Bellingham et al. 1992; Bellingham and Tanner 2000; Tanner and
202 Bellingham 2006; Tanner et al. 2014) and Hurricanes Ivan (2004), Dennis (2005) and Dean
203 (2007) (Luke et al. 2016a,b).
204
205 **Method and materials**
206 ***Reconstructing hurricane topographic exposure vulnerability***

207 Exposure vulnerability (EV) is a unitless measure that can be used to link the disparity in
208 hurricane exposure to the responses of tree species and the forest ecosystem at sites where there
209 is hurricane disturbance (Luke et al. 2016a). The calculation of EV requires hurricane tracks, a
210 digital surface model (DSM), and information on wind direction and speed (Luke et al. 2016a).
211 EV maps for three hurricanes (Ivan (2004), Dennis (2005) and Dean (2007)) were generated by
212 Luke et al. (2016a) and were used in this present study. Wind speed and direction data that were
213 used to construct the three EV maps were obtained from processed ultra-high-resolution images
214 of circular hurricane wind bands. These were created from QuikSCAT scatterometer satellite
215 data that were processed using a Scatterometer Image Reconstruction (SIR) technique (Early and
216 Long 2001). The images included colour-coded information on wind speed (in knots) overlaid
217 with wind flags, which point in the direction from which the wind is blowing (see: Luke et al.
218 2016a). However, QuikSCAT Scatterometer images (available at:
219 http://www.scp.byu.edu/data/Quikscat/HRStorms.html) are only available for the period 1999–
220 2009 for hurricanes that developed in the Atlantic Ocean and the Caribbean Sea. Therefore, in
221 the present study, we used a method modified from Luke et al. (2016a) to reconstruct EV maps
222 for hurricanes that preceded 1999 using information on wind speed and wind direction obtained
223 from proxy or surrogate images.
224
225 To reconstruct the EV maps of pre-1999 hurricanes, we first downloaded an ESRI point .shp file
226 of the tracks of all hurricanes recorded in the Caribbean from the National Oceanic and
227 Atmospheric Administration (NOAA), National Climatic Data Center website
228 (http://www.ncdc.noaa.gov/ibtracs/index.php?name=wmo-data) and the tracks were re-projected
229 to the Jamaican datum, JAD 2001. Tracks of hurricanes categorized as category 2, 3 and 4 using

the Saffir-Simpson Hurricane Wind Scale (maximum wind speed ≥ 154 km hr^{-1} at their eye as they passed at their closest points to the coastline of Jamaica) during the period 1852 to 1988 (Table 1), with centers that passed within 0–160 km of the northern or southern coastline of Jamaica, were then selected. A 160 km threshold was used because Hurricane Emily, which passed 160 km from the south coast (in 2005), had minimal effect on the JCM forest, as the outer bands that passed over the JCM had wind speeds < 65 km hr^{-1} (Luke et al. 2016a). Next, where possible, surrogate/proxy QuikSCAT images representing 'typical' category 2, 3 and 4 hurricanes over water in the Caribbean were selected and downloaded as a .gif file format and rectified to the Jamaican datum. These images included Hurricanes Michelle (November 3, 2001; wind speed: 167 km hr^{-1}; location: 18° N 84° W), Charley (August 12, 2004; wind speed: 148 km hr^{-1}; location: 20° N 81° W), Ivan (September 11, 2004; wind speed: 240 km hr^{-1}; location: 18° N 80° W), Jeanne (September 20, 2004; wind speed: 111 km hr^{-1}; location: 26° N 72° W), Emily (July 15, 2005; wind speed: 213 km hr^{-1}; location: 15° N 23° W), Dennis (July 7, 2005; wind speed: 167 km hr^{-1}; location: 18° N 75° W) and Dean (August 20, 2007; wind speed: 240 km hr^{-1}; location: 18° N 81° W). A list of hurricanes for which the EVs were reconstructed, and the proxy hurricane(s) used to model the EV of each hurricane are presented in Table 1. The best proxy image for Hurricane Gilbert was determined by comparing several proxy QuikSCAT images to a rectified satellite image of Gilbert as it passed over Jamaica. Hurricane Ivan closely matched the satellite image and was therefore used to model the final EV map of Hurricane Gilbert. The EV of Hurricane Gilbert was also modelled using proxy hurricanes from the same Saffir-Simpson Hurricane Wind Scale such as Hurricanes Emily and Dean, and the average of all three proxies (Ivan, Emily and Dean).

For each hurricane, the 'Georeferencing' function in ArcGIS was used to center the surrogate or proxy hurricane images on the approximate location of the hurricane's eye, specifically on track points found close to or over Jamaica. Wind flags found close to the JCM and BM were digitized as polylines in ArcGIS. For wind speeds ≥64 km hr^{-1}, the upper value/range of the wind bands that were likely to affect the BM and the JCM were used as estimates of wind speed. There were no wind speed values for the wind bands closer to the track points (that is, for wind speeds > 93 km hr^{-1}). Average wind speed was estimated for these wind bands by averaging the wind speed at the track point over which the image was centered and 93 km hr^{-1}, which was the maximum wind speed of the wind category below the > 93 km hr^{-1}category. The 'hillshade' feature in ArcGIS was used with a digital surface model (DSM; 6.5 m resolution) of the eastern section of Jamaica, to generate maps of topographic exposure to wind from various directions (following Mikita and Klimánek 2010 and Batke et al. 2014). The hillshade feature requires the input of an azimuth angle (wind direction) and an altitudinal angle (range 0⁻90°) (wind inflection angle). A fixed wind inflection angle of 20^{o} that was used by Luke et al. (2016a), was used to create the EV maps. Hillshade maps of exposure for each hurricane were generated by inputting the following formula from Luke et al. (2016a) into the raster calculator in ArcGIS:

$$\mathrm{EV} = (\sum_{i=1}^{n}(\text{wind speed}_i * \text{hillshade map of exposure}_i))/n,$$

where *i* is one of several locations where the surrogate/proxy hurricane image(s) was (were) centered and evaluated (e.g., location (*i*) = 1, 2, 3, 4…) and *n* is the total number of locations evaluated/hillshade maps created.

Permanent sample plot data from the Blue and John Crow Mountains

Data from the upper montane rain forest of the BM are from the "Tanner's plots" established in 1974 in four sites, within which are contiguous 10 × 10 m plots (Col [0.09 ha], Mor [0.06 ha], Mull [0.10 ha], and Slope [0.10 ha]; Tanner 1977). The plots were established within 300 m of each other, at elevations 1580–1600 m (Figures 1 and 6) and covered a total area of 0.35 ha. Although the plots are small in size and number, they sampled a representative area due to the low tree species diversity in the BM. Specifically, 33 species that were sampled in the plots in 2009 accounted for 93% and 95% of all the stems (≥ 3 cm DBH) and basal area, respectively (Chai et al. 2012). For a full description of the sites see Tanner (1977) and Tanner et al. (2014). All stems ≥ 3 cm diameter at breast height (DBH, measured at 1.3 m aboveground) were identified to species, scored as live or dead, and measured (DBH) in 1974, 1984, 1989, 1991, 1994, 2004, and 2009 (Tanner et al. 2014). When the plots were re-enumerated after Hurricane Gilbert in 1989 and 1991, visible signs of hurricane damage and modes of recovery were documented (i.e., percentage of all stems in the plots scored as defoliated, dead and resprouting; Bellingham et al. 1995) and these data were used in this study.

More extensive data from the BM were derived from the "Bellingham's plots", specifically, 16 permanent 200 m^2 circular plots covering a total area of 0.32 ha that were established in 1990, 20-23 months after Hurricane Gilbert, along five, 500-m transects, 1 km apart (Bellingham 1991) (Figures 1 and 7). The plots were established at elevations 1320–1920 m, and were located orthogonal to the Grand Ridge of the BM at distances of 0, 250 and 500 m along each transect, at the northernmost point, the top of the Ridge and the southernmost point, respectively (Bellingham 1991) (Figures 1 and 7). All stems, living and dead, that were ≥ 3 cm DBH were measured and identified and the plots were re-enumerated in 1994 and 2004. Types of damage

caused by Hurricane Gilbert and modes of recovery that were recorded included mortality, uprooting, breakage, crown defoliation and resprouting (Bellingham 1991). Damage and recovery (resprouting) were expressed as a percentage of all stems in the plots.

Table 1. Information on the hurricanes reconstructed in this study, including the date the first exposure vulnerability map for each hurricane was reconstructed, average wind speed or range of wind speeds at the eye, distance from the eye of the hurricanes to the closest point along the coastline of Jamaica, average cardinal direction (or angle) of the track of the eye of the hurricanes relative to the study sites (used in the Curve Fit and the *calc* polynomial regressions) and the proxy hurricanes used to reconstruct their exposure vulnerability.

Hurricane	Date	Wind speed (km hr^{-1})	Distance (km)	Angle (degrees)	Proxy hurricane(s)
1852 (unnamed)	06/10/1852	167	73.5	199.08	Jeanne
1880 (unnamed)	06/08/1880	148	71	195.81	Jeanne
1903 (unnamed)	11/08/1903	195	0	279.17	Jeanne
1912 (unnamed)	17/11/1912	93 - 185	0	336.14	Jeanne
1915 Galveston	13/08/1915	176	13.2	333.19	Jeanne
1951 Charlie	17/08/1951	139 - 176	0	202.08	Michelle, Charley and Dennis
1964 Cleo	25/08/1964	232	113.7	40.71	Michelle and Dennis
1980 Allen	06/08/1980	213	49	300.39	Ivan, Emily and Dean
1988 Gilbert	12/09/1988	204 - 213	0	215.75	Ivan, Emily and Dean
2004 Ivan	11/09/2004	241 - 250	40.3	203.44	Ivan
2005 Dennis	07/07/2005	185	45.9	40.82	Dennis
2007 Dean	20/08/2007	231	40.9	167.69	Dean

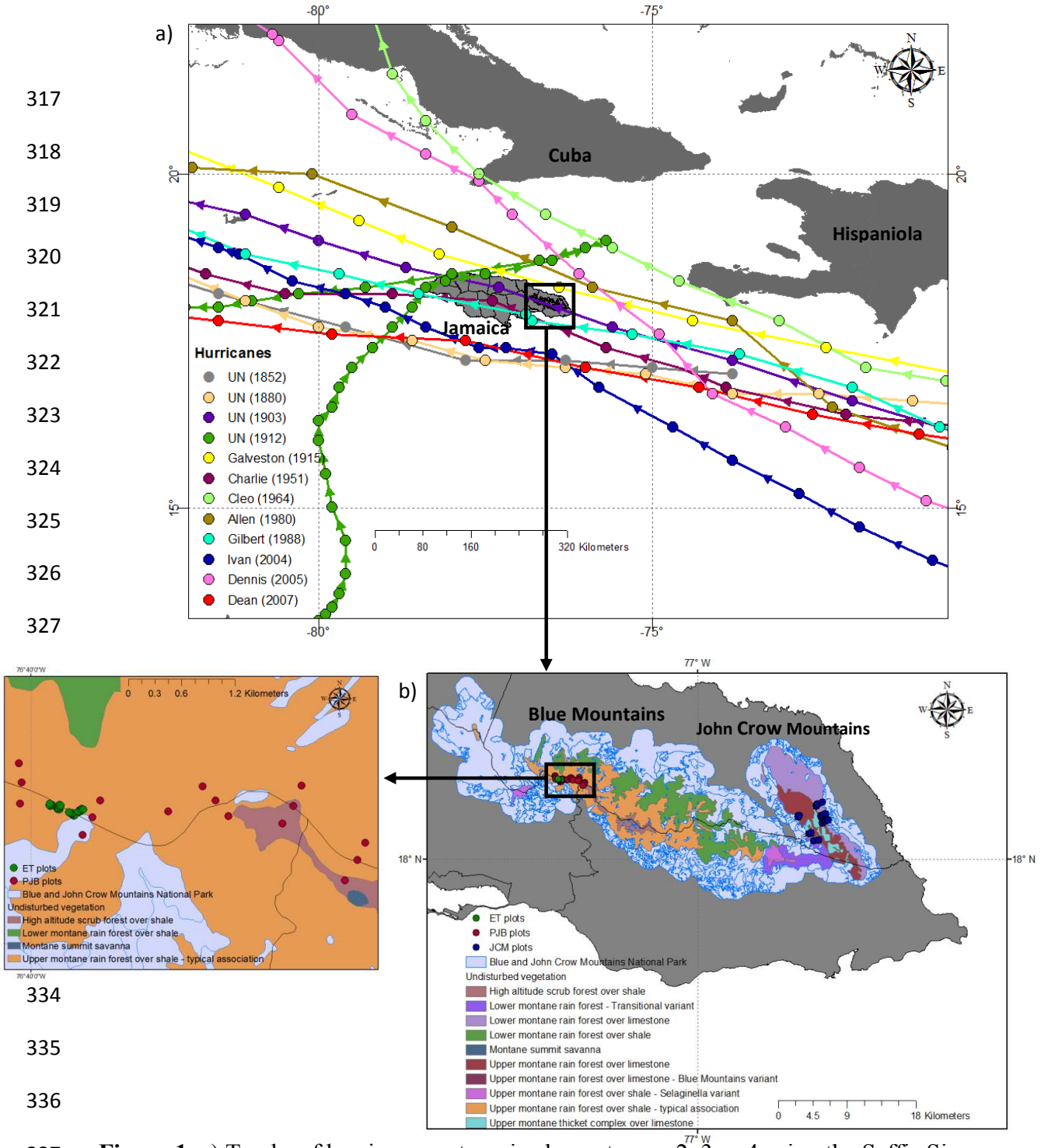

Figure 1. a) Tracks of hurricanes categorized as category 2, 3 or 4 using the Saffir-Simpson Hurricane Wind Scale, with centers that passed within 0–113 km of the northern or southern coastline of Jamaica during 1852–2007. Exposure vulnerability of these hurricanes was reconstructed. Also included are b) maps of the study site, the Blue and John Crow Mountains National Park (source: Muchoney et al. 1994), showing the extent of several old growth vegetation classes, and overlaid with the location of permanent sample plots (ET: Tanner (1977); PJB: Bellingham (1991) and JCM: Luke et al. (2016a)) established in the Blue and John Crow Mountains, Jamaica. The colour coded arrows show the direction of the hurricanes.

345

346 ***EV model evaluation data***

347 Luke et al. (2016a) used global site factor (GSF) (calculated from hemispheric photographs) data
348 collected six months after Hurricane Dean (in 2008) in PSPs located in the JCM to test how well
349 their EV model performed. Specifically, they used a spatially explicit generalized additive mixed
350 model (GAMM) to showed that the EV values, which were extracted from the EV maps using
351 the GSF plot location, explained the highest deviance in the GSF data and that GSF increased
352 significantly with Hurricane Dean EV (Luke et al. 2016a). In the present study, we used a similar
353 approach. In particular, we used a spatially explicit generalized linear mixed model (GLMM)
354 and damage and recovery data from Bellingham's and Tanner's plots to determine if the
355 reconstruction method accurately modelled sites that were exposed to Hurricane Gilbert.
356 Dependent variables used in the GLMM included percentage of stems in the plots that died, had
357 crown defoliation, and had resprouted in 1990 from Bellingham's plots. From Tanner's plots, the
358 dependent variables included percentage of stems with crown defoliation and resprouting in 1989
359 and 1991.

360

361 Based on previous stand-level assessments (Bellingham 1991), it was expected that plots with
362 the highest exposure would suffer greater hurricane damage and show evidence of a higher
363 percentage of recovering stems. Nevertheless, we evaluated the influence of several independent
364 variables on the damage and recovery data to determine if EV was the most important predictor.
365 As such, the independent variables included elevation, aspect, topographic position index (TPI)
366 and EV values for Hurricane Gilbert, which were extracted at each plot location. Elevation
367 values were obtained from the DSM, whereas aspect and TPI values were extracted from maps

368 that were generated from the DSM. The TPI map was generated using the Land Facet Corridor
369 Designer Tools for ArcGIS 10 (Jenness et al. 2013). TPI values are continuous and as they
370 change from negative to positive this is indicative of a transition from valleys to slopes to ridge
371 tops. Specifically, negative TPI values represent valleys and gullies, TPI values near zero
372 represent mid-slopes, and positive and comparatively large TPI values represent ridges and ridge
373 tops (Jenness et al. 2013). To determine the effects of hurricane proxy choice (Hurricane Dean
374 QuikSCAT Scatterometer image) on EV map accuracy, the model evaluation was repeated for
375 Gilbert EV maps reconstructed using other proxies such as Hurricanes Dean and Emily and
376 average EV of the three proxy hurricanes. The accuracy of EV maps generated using the best
377 single proxy, which was Hurricane Ivan, a proxy from the same Saffir-Simpson Hurricane Wind
378 Scale category, which is Hurricanes Dean and Emily, and the average of the three proxies, was
379 then compared. The statistical method used to evaluate the EV model is described below.
380
381 ***Aggregating the spatial patterns of hurricane disturbance: modelling the influence of***
382 ***hurricane direction and distance on exposure vulnerability***
383 Unless stated otherwise, statistical tests were performed using the R programming language (R
384 Development- Core-Team, 2017). The path of the hurricane is determined by the storm forward
385 speed and direction. Both influence the angle of approach of the hurricane to an island or a
386 landmass and the cardinal direction of the track of the hurricane. Bivariate plots of EV and
387 aspect were therefore generated and inspected, and were used to determine the directional
388 patterns of exposure based on the cardinal direction/angle of the track of a hurricane's eye.
389 Before the data were plotted, a raster image of undisturbed upper montane forest in the BM
390 (Figure 1) was converted to a point .shp file. This was used to extract EV and aspect values from

391 the respective maps. The *polarPlot* function from the 'openair' package (Carslaw and Ropkins,
392 2012) was then used to construct a bivariate plot of the relationship between EV and aspect for
393 each hurricane. This process involves creating a smooth surface by fitting a generalized additive
394 model (GAM) to the data. The level of smoothness is controlled by the smoothing parameter *k*
395 and we used the default value (100). The *polarPlot* function and the resultant bivariate plot are
396 suitable for a graphical analysis but not for quantitative purposes. As such, directional
397 information on EV was discerned graphically when the smooth surface was plotted in polar
398 coordinates. Plots for the JCM were very similar to those of the BM, and therefore, they are not
399 presented. The relationships between the cardinal direction of the tracks of the eyes of the
400 hurricanes relative to the study sites and EV and distance from the eyes of the hurricanes to
401 the study sites and EVwere then explored (Figures 5-8). A polynomial (2nd-degree) model was
402 found to be the most suitable model for representing this relationship. As such, a pixel-level
403 (2nd-degree) polynomial regression analysis was conducted using the USGS Curve Fit extension
404 for ArcMap (De Jager and Fox, 2013). This was used to map the spatial patterns of exposure
405 based on the angle or cardinal direction of the track the hurricane's eye and distance to the
406 hurricane's eye, over the period 1852–2007. Curve Fit uses a linear or nonlinear regression to
407 calculate a unique mathematical model at each pixel of the input raster data sets (De Jager and
408 Fox, 2013). The input for the Curve Fit function included a time series of EV maps for the BM
409 and JCM (dependent variable), and the average angle or cardinal direction (in degrees) of the
410 track of the eye of each hurricane relative to the study sites or the distance to the eye of each
411 hurricane from the study sites, as an independent variable (Table 1).
412

413 Before the exposure maps were added to the Curve Fit function, they were first clipped to an area
414 of interest that included only natural old growth (including old secondary) forest of the
415 predominant forest type found at both sites where the plots were established (Figure 1). This
416 helped to reduce processing time. The Curve Fit output products generated for this study
417 included the P-value, adjusted R^2 and parameter a2 of the fitted polynomial regression, as image
418 files. The a2 parameter is the regression coefficient for the squared term. If $a2 > 0$, then the
419 relationship with the response is convex or concave upward, whereas if $a2 < 0$, then the
420 relationship is concave downward. The *calc* function in R can be used to generate similar outputs
421 and this was used to generate maps from a fitted pixel-level polynomial regression for the period
422 1852-1988. At each plot location, these values (from the Curve Fit image files) were extracted
423 and used in subsequent analyses. Bellingham's plots were likely to be influenced by hurricanes
424 that struck the island before the final census was conducted in 2004; therefore, only values from
425 the *calc* image files were extracted and used. Although adjacent pixels would likely influence the
426 EV value of a pixel, the pixel-level regression only considers a single pixel at a time and
427 generates a model for each pixel. Consequently, there was no spatial autocorrelation, but the data
428 were likely to be temporally autocorrelated. We therefore used the partial autocorrelation
429 function (PACF) and the autocorrelation function (ACF) to assess the residuals from polynomial
430 models developed using EV data extracted using the plot data to confirm that there was no
431 temporal autocorrelation, that is, they followed a white noise (random) process.
432
433 ***Bayesian hierarchical spatiotemporal/spatial model structure: EV model evaluation and the***
434 ***effects of EV and/or topographic features on tree diversity and density***

435 Tanner's plots were established according to a nested design, which included several contiguous
436 subplots nested within four plots or 'sites'. Also, the layout of Bellingham's plots followed a
437 fully systematic design and Luke et al.'s (2016a) plots followed a structured or a stratified
438 randomized block design. Consequently, Tanner's subplots were spatially pseudo-replicated and
439 auto-correlated because they were adjacent to each other in space. Additionally, the plots within
440 each transect of Bellingham (1991) and within each block of Luke et al. (2016a) were also close
441 enough to each other to potentially be spatially auto-correlated. Nested, systematic and structured
442 data can be fitted in a standard linear model with nested, systematic, that is, using each transect
443 as a block, and structured fixed effects. However, the degrees of freedom must be adapted to the
444 design of the study, because the errors will likely be spatially correlated and thus violating the
445 assumption of independent observations or errors. This must be accounted for by a model to
446 obtain accurate mean sum of squares (Gelman 2005; Schielzeth and Nakagawa 2013). As such,
447 data from the nested subplots, the transects and structured plots can only be appropriately
448 modelled using mixed effects models, which cluster the data in groups as a random effect
449 (Schielzeth and Nakagawa 2013; Zuur et al. 2017) and estimate the standard errors correctly
450 (Gelman 2005), because the latter will be biased if they are not corrected for clustering. A better
451 approach is to use a mixed-model with a spatial autocorrelation structure (using the coordinates
452 of the center of the subplots and plots), as the errors are allowed to be correlated and/or to have
453 unequal variances (Crawley 2012). However, some of the data were also likely to be temporally
454 auto-correlated; as a result, the most appropriate models should include spatial and temporal
455 autocorrelation structures. Nonetheless, the choice of frequentist methods that can cope with
456 these structures is limited, and the most appropriate methods require Bayesian statistics (Zuur et
457 al. 2017). Consequently, the models that were developed in this study were fitted using a

458 Bayesian approach based on the Integrated Nested Laplace Approximation (INLA), implemented
459 using the 'INLA' package (Rue et al. 2009; Lindgren et al. 2011; Martins et al. 2013; Lindgren
460 and Rue 2015; Rue et al. 2017). The method was used due to its flexibility (see below) and
461 because the posterior marginal probabilities are approximated more efficiently and faster, when
462 compared with traditional MCMC approaches (Rue and Martino 2007; Rue et al. 2009).
463
464 Two types of model were developed: models with either a spatiotemporal random effect for
465 overall assessments, regardless of time, and models with a spatial random effect for each
466 individual census. Models were developed for EV model evaluation and to determine whether
467 average EV from several hurricanes, topographic parameters or data from the Curve Fit and the
468 *calc* function output products could be used to explain spatial and/or spatiotemporal patterns of
469 tree diversity and density in the BM and JCM. For the JCM, Luke et al. (2016a) reported the
470 results of assessments of the Shannon–Wiener (H') diversity index versus EV and topographic
471 parameters for individual censuses. As such, in the present study, only the influence of the Curve
472 Fit output products was checked for the individual census periods. The models were developed
473 following a spatially explicit generalized linear mixed model (GLMM) framework. The response
474 variable at a given plot location and census interval was assumed to have a distribution that
475 belonged to the exponential family. As such, suitable distributions and link functions were
476 chosen for the response variables. For the EV model evaluation exercise, the response variables
477 were expressed as a percentage of the stems found in each plot (percentage defoliated, resprouted
478 and dead stems) and as such, either a binomial (BIN), or a zero-inflated binomial Type 0 (ZIB.0)
479 with a logistic link function was used. The ZIB.0 was chosen if the data had four or more zero
480 values and it was deemed a better fit. The dependent variables in the other models were either H'

values or density values for each plot that was sampled during the periods 1974-2009 (Tanner's plots), and 1991-2004 (Bellingham's plots) in the BM, and 2006-2012 (Luke et al.'s (2016a) plots) in the JCM. For H' values derived from Tanner's plots, a Gaussian distribution was used. A Gamma distribution and log-link function were used for H' and density values derived from Bellingham's and Luke et al.'s (2016a) plot data. A value of 0.00001 was added to the density values, because a Gamma distribution does not include zeros.

The parameters of the chosen exponential family (ϕ) were linked to a structured additive predictor η through their canonical link function $g(\cdot)$, such that $g(\phi) = \eta$. The linear predictor was defined as:

$$\eta = \beta_0 + \beta_1 * Var.1 + \beta_2 * Var.2 + f(Var.3) + f(s,t)$$

where η was the linear predictor for any one of the response variables, β_0 was the intercept, β_1 and β_2 were the regression coefficients for the predictors *Var.1* and *Var.2*, and *Var.3* was also a covariate/predictor. In general, the semiparametric function $f(\cdot)$ can be used either to relax the linearity of the covariates/predictors, that is smooth effects similar to a GAM, or it can be used to define either the spatial or spatiotemporal random effect (Rue et al., 2009). In this study, $f(\cdot)$ was used to model the smooth, non-linear effects of some covariates/predictors using either a first-order or second-order random walk process (RW1 or RW2) given by $f(Var.3)$. A polynomial INLA spatiotemporal model was used to confirm that there was a non-linear relationship between the response and the predictor before smoothing was applied, i.e. that all the degrees or the orders of the polynomial were important. The $f(\cdot)$ was also used to represent the effects of the spatial position of each plot location (using the coordinates taken at the center of each plot) by allowing for the inclusion of a spatially structured random effect $f(s)$, and for the spatiotemporal

504 models this followed an autoregressive process $f(s,t)$. The latter represented a Matérn correlation
505 structure but with a different realization every year (Cosandey-Godin et al. 2014).
506
507 The spatially-structured random effect was modeled by a Gaussian random field (GRF) using the
508 stochastic partial differential equation (SPDE) approach of Lindgren et al. (2011). A GRF with a
509 Matérn covariance function can be represented as a Gaussian Markov Random Field (GMRF)
510 (Lindgren et al. 2011). A GMRF is a spatial process that models the spatial dependence of data
511 observed on a regular grid, lattice or geographic region (Cameletti et al. 2013). The SPDE
512 approach is used to find a GMRF with local neighbourhood and sparse precision matrix **Q** (i.e.,
513 the inverse of the covariance matrix) that best represents the Matérn field (Lindgren et al. 2011),
514 to avoid the "big n problem" that occurs with large spatiotemporal datasets (Banerjee et al 2004).
515 The SPDE method achieves this by allowing for the evaluation of the continuous GRF as a
516 discretely-indexed random process (i.e. a Gaussian Markov Random Field; Lindgren and Rue
517 2015). In particular, the SPDE method subdivides the domain, in this case the area of interest
518 where the plots were established (the forests of the BM and JCM), into non-intersecting triangles
519 creating an index mesh, instead of a regular grid (Lindgren et al. 2011). Linear combinations of
520 basis functions, defined on the locations of the set of vertices, are used in the triangulation to
521 represent the field (Lindgren et al. 2011). The meshes that were used to approximate the spatial
522 fields for the BM and JCM are shown in Appendix S1. The meshes were confined to the area of
523 interest for both sites. Different mesh sizes were used for both sites, including a mesh that only
524 encompassed the plot locations. This was gradually extended to include the entire study area for
525 each site. Also, the mesh should typically be extended beyond the study area to reduce boundary
526 effects where the variance is twice as large as inside the domain. For this study, the final mesh

used for either site yielded very similar results as the mesh size increased. As such, the final mesh that was bounded by the area of interest was used. For a more detailed explanation of the SPDE approach see Lindgren et al. (2011).

The sampling times for Tanner's and Bellingham's plot censuses were unequally spaced, so for the models they were treated as data collected over a continuous time domain and were discretized over a set of knots, with equal spacing over the sample period. When applying models with spatial correlation, a 2-D mesh is defined (Zuur et al. 2017). When knots are used, a 1-D mesh that is dependent on knot values is constructed (Zuur et al. 2017) and, similar to the spatial model, piecewise linear basis functions are used, but at a set of time knots (Krainski et al. 2017). The knot values are used to calculate weighting factors that are inversely proportional to the distance between the sampling year and the knots (Zuur et al. 2017). To fit the space-time continuous model, the time knots and the temporal mesh need to be determined. Specifically, the seven and three sample times for Tanner's and Bellingham's plot data were discretized over four and three knots, respectively (Appendix 1). For Tanner's plots, the knots represented the years 1974, 1985.7, 1997.3 and 2009, whereas for Bellingham's plots, the knots represented the years 1990, 1997 and 2004. The final model was specified as a SPDE model for the spatial domain and an AR(1) model for the time dimension. This model allowed for the simulation of the conditional marginal distribution at each time, that is, it simulated a realization of the spatial random field for each time. Two space-time models were used: one for discrete time domain (two years for the JCM) and for the second model, time was discretized over a set of knots (for the BM).

549 Before the statistical tests were performed, significantly correlated independent variables (with a
550 correlation > 0.5) were identified using Spearman's rho statistic and test. The Deviance
551 Information Criterion (DIC), which was computed by R-INLA, was used to compare the
552 goodness-of-fit of the models. The DIC is comparable to the Akaike Information Criterion
553 (AIC), but it is more suitable for hierarchical Bayesian models (Spiegelhalter et al. 2002).
554 Models with the lowest DIC values were generally considered as the best models. In addition,
555 the marginal R-squared (following Zheng (2000)) was calculated as follows:
556 $100*(1 - (\sum_{t=1}^{t}\sum_{n=1}^{n}(depend - fitted)2 / \sum_{t=1}^{t}\sum_{n=1}^{n}(depend - \text{mean}(depend))2))$,
557 where *t* is time when *n* subjects were considered, *depend* is the response variable, and *fitted* is the
558 values predicted by the model. The most parsimonious final models that included independent
559 variables, which were not significantly correlated, were identified and reported. Model fit was
560 also evaluated using scatter plots of the observed and predicted data and quantile-quantile
561 residual plots. In addition, INLA performs a 'leave out one' cross-validation from which two
562 indices that can be used to evaluate model predictive performance are computed (Blangiardo and
563 Cameletti 2015): the probability integrity transform (PIT) (Dawid 1984) and the conditional
564 predictive ordinate (CPO) (Pettit 1990). The empirical distribution of the PIT can be used to
565 evaluate model predictive performance (Gneiting et al. 2007). If a histogram of the PIT values
566 follows a uniform distribution, this means that model predications are coherent with the observed
567 data (Blangiardo and Cameletti 2015). In addition, when the PIT and CPO indexes are computed,
568 numerical problems can occur (Held et al. 2010). The 'failure' vector automatically provided by
569 INLA contains a value of 0 or 1 for individual observations (Blangiardo and Cameletti 2015). A
570 value of 1 indicates that for a particular observation, the predictive measures are not reliable due
571 to some problems with the calculation (Blangiardo and Cameletti 2015). If the vector is summed,

572 a value of 0 indicates that no failures were detected. Final models were not selected unless the
573 sum of the CPO was equal to 0 and a histogram of the PIT values showed a uniform distribution.
574
575 In most cases, the default and recommended priors were used; specifically, vague priors or
576 estimations of non-informative priors (Cosandey-Godin et al. 2014). However, to avoid
577 overfitting, the penalized complexity prior (PC-prior) framework was adopted. A PC-prior
578 derived by Fuglstad et al. (2019) was used to define the model parameters of the SPDE model as
579 the practical range and the marginal standard deviation. It is weakly informative, and complexity
580 is penalised by shrinking the range to infinity and the marginal variance to zero (Fuglstad et al.
581 2019). For the SPDE, the PC-prior ensured that the spatially structured effect operated at a
582 similar but not smaller spatial scale as the model covariates/predictors. Otherwise, the spatial
583 effect would explain the data better than the covariates, rendering the model meaningless while
584 inflating model accuracy and the marginal R-squared and deflating the DIC, rendering them
585 useless for model selection. Several values for the range were used (starting with half the
586 distance between the farthest points), until there was no overfitting. A PC-prior, developed by
587 Simspon et al. (2017), was also considered for the random walk processes (RW1 and RW2). It
588 requires defining a reference standard deviation σ_0 and the right-tail probability u, as $P(\sigma_0 > \sigma) =$
589 u (Simspon et al. 2017). The PC-prior controlled the level of smoothness and a value of 1 for σ_0
590 is the suggested starting point. Using lower values will result in a smoother fit and progressively
591 lower values will give a straight line.
592
593 Before the models were accepted, several ways in which EV could be used to explain
594 spatiotemporal trends were first explored. Average 'legacy' EV calculated from multiple

hurricanes that affected a site before a census, with no adjustment for time (since each hurricane affected the sites/plots), was found to be the best predictor of diversity in the JCM (Luke et al. 2016a). In the present study, we found that average 'legacy' EV was more suitable for assessing the overall effects of EV when multiple re-numeration times were used in the models (Figure 9). However, we used a manual stepwise forward selection approach to identify the best or most suitable hurricanes and the number of hurricanes for averaging. Specifically, EV values for each hurricane were first included in a regression model with a response variable (diversity or density), and important EVs were identified. The two most important EVs (based on DIC and the marginal R-squared values) were then averaged and model fit, that is the DIC and the marginal R-squared values, was assessed. If model fit was improved by averaging the two most important hurricane EVs, that is if the DIC decreased and the marginal R-squared increased, additional EVs were then included in the average. If model fit did not improve when the EV of a hurricane was included in the average, it was dropped. This was repeated until an average 'legacy' EV that yielded the lowest DIC and the highest marginal R-squared values was identified. This was then used to identify the most parsimonious model.

The most parsimonious final models were identified using a manual stepwise backward selection approach and were reported. Specifically, important predictors with the highest marginal R-squared and the lowest DIC were identified, and other predictors that were correlated with these predictors but had a lower marginal R-squared and higher DIC were dropped. If there were > 1 uncorrelated predictors, they were all included in a model and the final model was accepted if they were all important. If one or more of the predictors were not important when they were added to the model, they were dropped until the most parsimonious model was identified. These

618 models yielded the lowest DIC, the highest marginal R-squared and included independent
619 variables that were not significantly correlated.
620
621 **Results**
622 The nominal range, which is the minimum distance at which data from two plot locations are
623 uncorrelated (or correlation between the two plots is ≤ 0.1), varied for the models that were used
624 to analyze plot data from the two study sites. For all the models that included Tanner's plot data,
625 the nominal range was 5.1–8.2 km, for Bellingham's plot data 4.7–8.4 km and for Luke et al.'s
626 (2016a) plot data 5.9–8.4 km (Tables 2–8). For the assessments (e.g. EV versus tree diversity or
627 density) that included all the censures (i.e. assessing the overall effects regardless of time), the
628 data used were not found to be temporally auto-correlated; but in all cases model fit improved
629 with the inclusion of spatiotemporal random effects. In addition, for all models, the variance of
630 the spatial effect was lower than that of the model variance (Tables 2–8).
631
632 ***EV model evaluation***
633 For the BM, damage and recovery data from Bellingham's plots, in particular completely
634 defoliated and reprouting stems, were found to increase significantly with Hurricane Gilbert EV
635 (Figure 2a,b; Table 2), with marginal R-squared (mR^2) values of 37.5% and 47.1%, respectively
636 (Table 2). This indicated that the method used to reconstruct the EV of past hurricanes generated
637 maps of EV that can be considered as a proxy to damage caused by these hurricanes. In addition,
638 the best proxy for Hurricane Gilbert, that is an EV map created using metrological data from a
639 processed QuikSCAT Scatterometer image of Hurricane Ivan, could be used to explain the
640 damage and recovery data from Bellingham's plots. Average EV from three proxies (Hurricanes

641 Emily, Ivan and Dean; mR^2 = 36.2%), and the other proxies (mR^2 = 30.1% (Dean) and mR^2 =
642 27.2% (Emily)) could only be used to explain the recovery data (Figures 2c–e; Table 2).
643 Therefore, in the absence of a single 'best' proxy, proxy images of other hurricanes from the
644 same Saffir-Simpson Hurricane Wind Scale category or the average of three proxies from the
645 same wind scale category, could, at the very least, be used to represent forest recovery from
646 hurricanes. The percentage of dead stems was better explained by elevation, that is dead stems
647 increased with elevation (mR^2 = 44.6%) (Figure 2f; Table 2). If data from Tanner's plots were
648 used, defoliated stems showed an S-shaped non-linear relationship with TPI (mR^2 = 66.1%),
649 indicating that the topographic location of the plots had a greater influence on hurricane damage
650 than was the case for Bellingham's plots, and in this case, damage was highest at or near ridge
651 crests (Figure 2g; Table 3). A similar pattern was reported by Bellingham et al. (1992) and
652 Tanner et al. (2014). Similarly, resprouting in 1989 and 1991 was explained by TPI being highest
653 at or near ridge crests (mR^2 = 40.3 and 60.8%, respectively) (Figure 2h & j; Table 3).
654
655
656
657
658
659
660
661
662
663

664

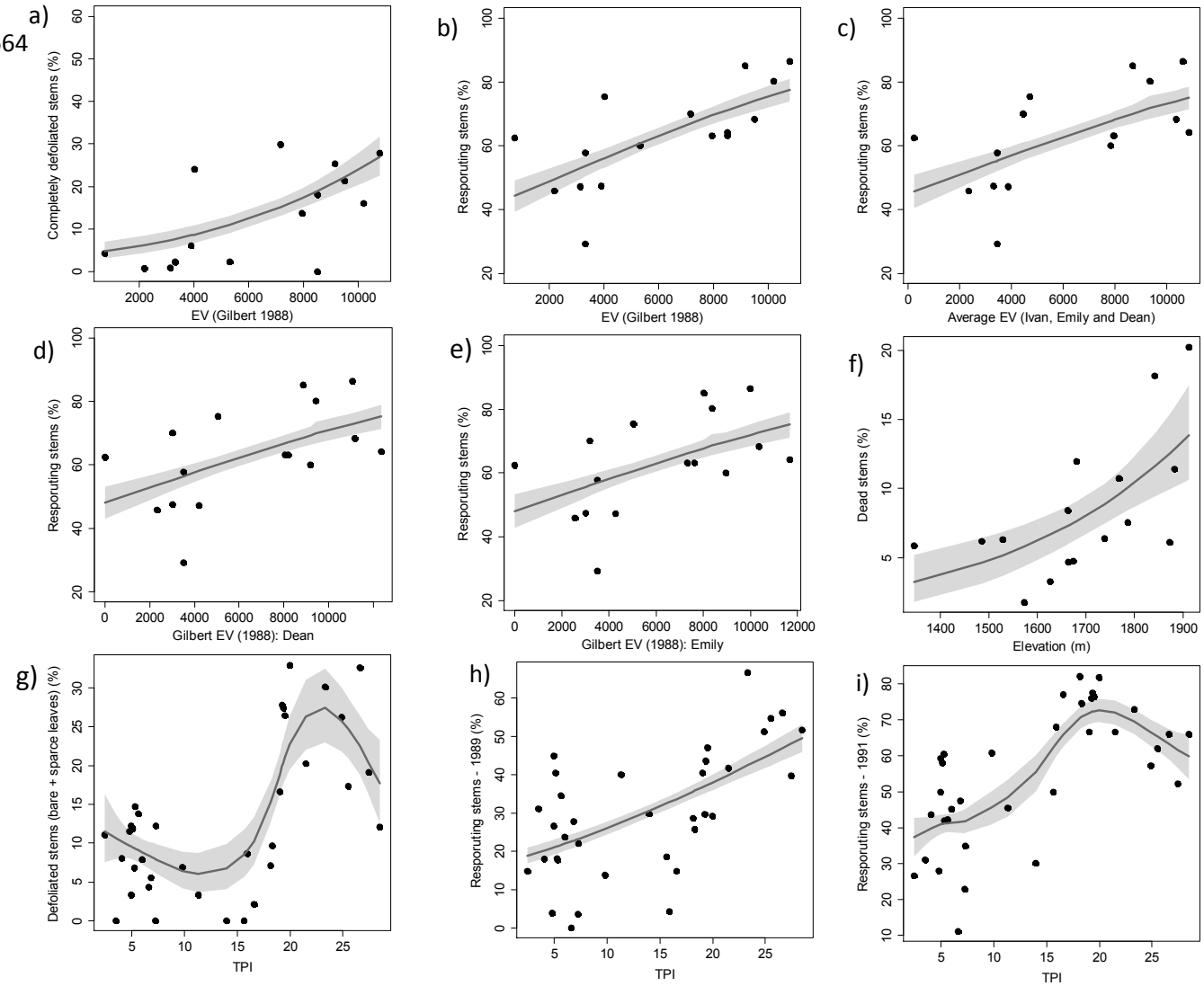

Figure 2. Observed (closed circles) and posterior mean predicted values (solid lines) and the 95% credible intervals (shade) obtained from hierarchal Bayesian spatial models used to assess the relationship between damage and recovery data obtained from Bellingham's (a–f) and Tanner's (g–i) plots several months after the passage of Hurricane Gilbert in 1988, and the reconstructed Hurricane Gilbert exposure vulnerability (EV) based on three proxy hurricanes (in the order of model fit: Ivan, the average of all three hurricanes, Dean and Emily) and other topographic parameters (elevation and topographic position index (TPI)).

665
666
667
668
669
670
671

672 **Table 2**. Summary of the marginal posterior distribution for model parameters obtained from
673 hierarchical INLA Bayesian models used to assess the relationship between damage and
674 recovery data from Bellingham's plots and Hurricane Gilbert exposure vulnerability (EV),
675 reconstructed using several proxy hurricanes including Hurricanes Ivan (2004), Dean (2007),
676 Emily (2005) and average (mean) EV from all three proxies that were found to be the most
677 important predictors (95% credible intervals did not contain zero) of damage and recovery in the
678 montane forest of the Blue Mountains, Jamaica, after the passage of Hurricane Gilbert in 1988.

Year	Variable	Parameters	Mean	$Q_{0.025}$	$Q_{0.975}$	mR^2	DIC	Priors
1989	Completely defoliated stems (%) ZIB.0	Intercept	-3.2	-3.6	-2.7	37.5	155.7	
		Glibert (Ivan)	0.0002	0.0001	0.0003			
		obs.var	6.7	2.5	17.5			
		spde.var.nom	0.0000295	-0.0000004	0.0002002			0.0023, 0.5
		spde.range.nom	6.5	0.7	30.8			3.9, 0.5
1989	Resprouting stems (%) BIN	Intercept	-0.3	-0.6	-0.1	47.1	159.2	
		Glibert (Ivan)	0.0001	0.0001	0.0002			
		spde.var.nom	0.0000196	-0.0000004	0.0001245			0.0023, 0.5
		spde.range.nom	8.1	0.7	41.3			3.9, 0.5
1989	Resprouting stems (%) BIN	Intercept	-0.19	-0.42	0.06	36.2	178.1	
		Glibert (Mean)	0.0001	0.0001	0.0002			
		spde.var.nom	0.0000197	-0.0000005	0.0001238			0.0023, 0.5
		spde.range.nom	8.2	0.8	42.0			3.9, 0.5
1989	Resprouting stems (%) BIN	Intercept	-0.07	-0.28	0.19	30.1	187.8	
		Glibert (Dean)	0.0001	0.0001	0.0001			
		spde.var.nom	0.0000251	-0.0000004	0.0001666			0.0023, 0.5
		spde.range.nom	7.4	0.7	36.6			3.9, 0.5
1989	Resprouting stems (%) BIN	Intercept	-0.06	-0.29	0.30	27.2	192.5	
		Glibert (Emily)	0.0001	0.0001	0.0001			
		spde.var.nom	0.0000277	-0.0000004	0.0001863			0.0023, 0.5
		spde.range.nom	7.1	0.7	34.3			3.9, 0.5
1989	Dead stems (%) BIN	Intercept	-7.2	-9.6	-5.0	44.6		
		Elevation	0.0028	0.0015	0.0042			
		spde.var.nom	0.0000194	-0.0000004	0.0001235			0.0023, 0.5
		spde.range.nom	7.3	0.7	35.7			3.9, 0.5

679 $Q_{0.025}$, and $Q_{0.975}$ = quantiles of the credible interval; DIC = Deviance Information Criterion; mR^2 =
680 marginal R-squared; ZIB.0 = zero inflated binomial Type 0 likelihood; BIN = Binomial likelihood;
681 obs.var = model variance; spde.var.nom = nominal spatial variance (priors = prior marginal standard
682 deviation and right tail probability); spde.range.nom = nominal spatial range (km) (priors = practical
683 range and right tail probability).

684
685
686
687
688

689 **Table 3**. Summary of the marginal posterior distribution for model parameters obtained from
690 hierarchical INLA Bayesian models used to assess the relationship between damage and
691 recovery data from Tanner's plots and topographic parameters (topographic position index (TPI))
692 that were found to be the most important predictors (95% credible intervals did not contain zero)
693 of damage and recovery in the montane forest of the Blue Mountains, Jamaica, after the passage
694 of Hurricane Gilbert in 1988.

Year	Variable	Parameters	Mean	$Q_{0.025}$	$Q_{0.975}$	mR^2	Priors
1989	Defoliated stems (%)	Intercept	-1.94	-2.06	-1.82	66.1	
	ZIB.0	obs.var	183.4	7.5	964.5		
	RW2	TPI.var	0.13	0.04	0.30		0.1, 0.05
		spde.var.nom	0.0000183	-0.0000004	0.0001149		0.0023, 0.5
		spde.range.nom	8.2	0.8	42.0		3.9, 0.5
1989	Resporuting stems (%)	Intercept	-1.60	-1.76	-1.44	40.3	
	ZIB.0	TPI	0.06	0.05	0.06		
		obs.var	44.1	8.1	166.3		
		spde.var.nom	0.0000406	-0.0000007	0.0002875		0.0023, 0.5
		spde.range.nom	5.3	0.5	23.4		3.9, 0.5
1991	Resporuting stems (%)	Intercept	0.20	0.13	0.28	60.8	
	ZIB.0	obs.var	183.4	7.5	964.5		
	RW2	TPI.var	0.027	0.009	0.061		0.03, 0.05
		spde.var.nom	0.0000379	-0.0000005	0.0002664		0.0023, 0.5
		spde.range.nom	5.1	0.5	22.3		3.9, 0.5

695 $Q_{0.025}$ and $Q_{0.975}$ = quantiles of the credible interval; mR^2 = marginal R-squared (%); RW2 = second-order
696 random walk process (predictor variance is followed by .var, e.g., TPI.var for RW2 and Prior = reference
697 standard deviation and the right tail probability); ZIB.0 = zero inflated binomial Type 0 likelihood;
698 obs.var = model variance; spde.var.nom = nominal spatial variance (Priors = prior marginal standard
699 deviation and right tail probability); spde.range.nom = nominal spatial range (km) (Priors = practical
700 range and right tail probability).

701

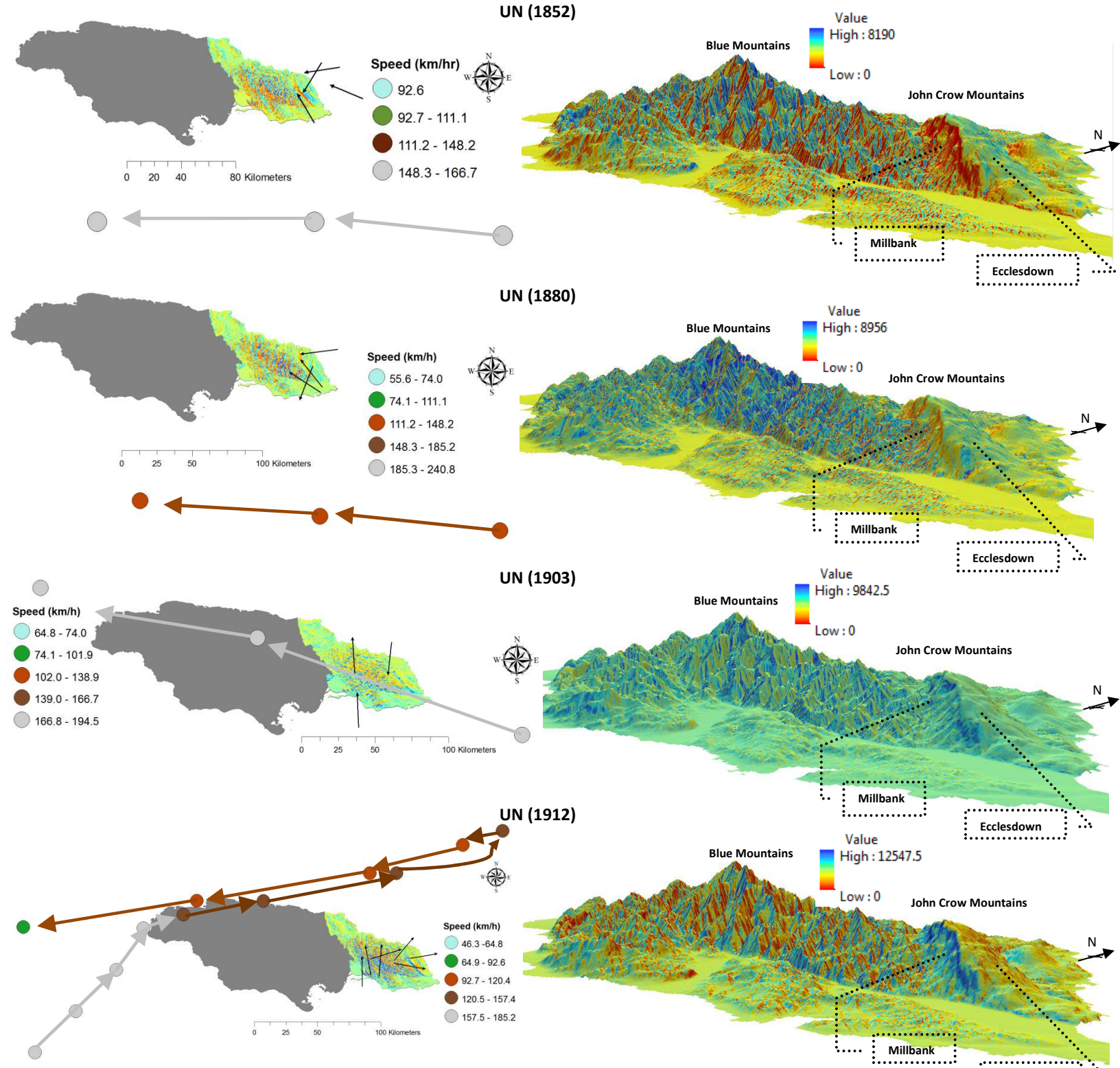

Figure 3. Exposure vulnerability (EV) maps (three-dimensional view) for category 2, 3 or 4 hurricanes, with centers that passed within 0–113 km of the northern or southern coastline of Jamaica, during the period 1852–1988. The two-dimensional inserts include hurricane tracks and direction (closed circles with arrows) with information on wind speed at each track location and wind direction (black arrows). Value = highest and lowest EV values. UN = unnamed hurricane.

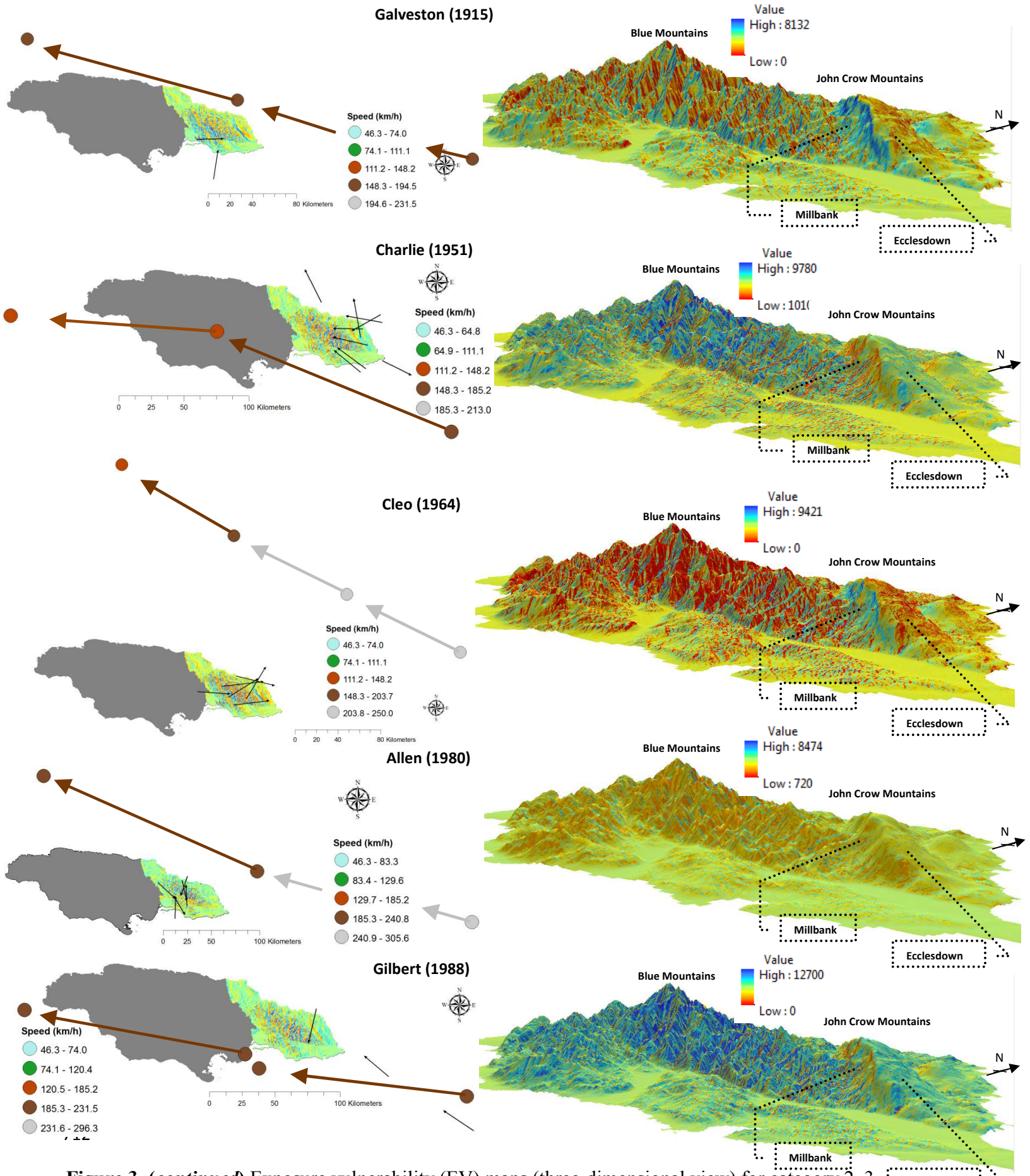

Figure 3. **(*continued*)** Exposure vulnerability (EV) maps (three-dimensional view) for category 2, 3 or 4 hurricanes, with centers that passed within 0–113 km of the northern or southern coastline of Jamaica, during the period 1852–1988. The two-dimensional inserts include hurricane tracks and direction (closed circles with arrows) with information on wind speed at each track location and wind direction (black arrows). Value = highest and lowest EV values. UN = unnamed hurricane.

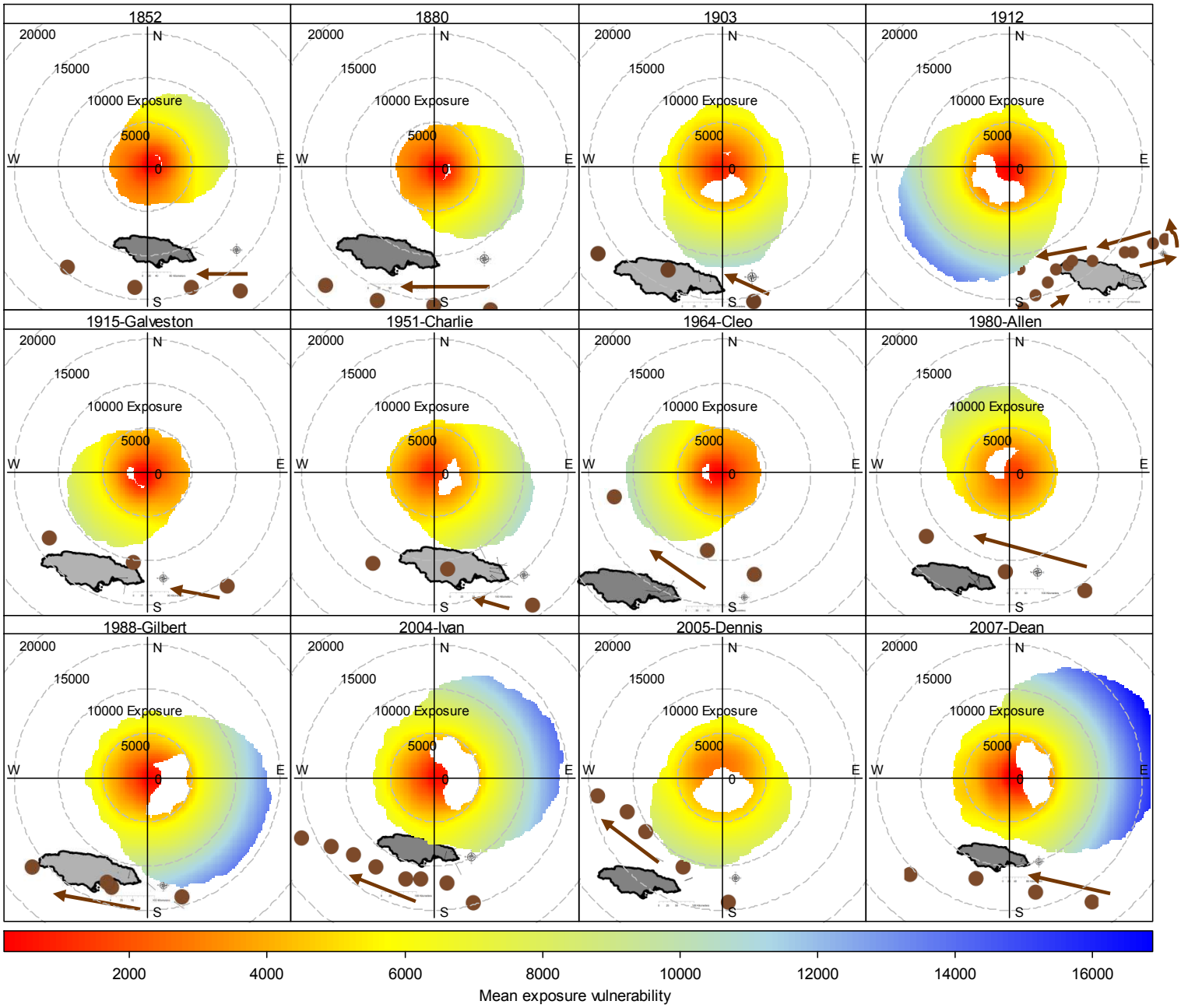

713 **Figure 4**. Bivariate polar plots (in polar coordinates) of aspect and exposure vulnerability (EV or
714 Exposure) for each hurricane with insert maps showing hurricane tracks (brown closed circles)
715 relative to the island of Jamaica. The polar plots show the aspect (or direction) with the highest
716 and lowest EV values when each hurricane affected the Blue Mountains. Arrows show the
717 direction of the hurricane tracks. The map inserts were placed where they can be viewed.

718

719

720

Long-term exposure in the Blue and John Crow Mountains

EV was found to be directional depending on the angle or cardinal direction of the track of the eye of each hurricane as it passed relative to the two study sites (Figures 3 and 4). If the track of a hurricane's eye passed the sites at angles or cardinal directions ranging from 279° to 41°, it passed along a trajectory from north-east to north-west of the study sites if it made landfall, or if it passed along the northern coastline (Figures 1, 3 and 4; Table 1). Due to the counter-clockwise rotation of hurricane winds, this resulted in southern to western aspects being more exposed (Figure 4). If the track of a hurricane's eye passed the sites at angles or cardinal directions ranging from 167° to 216°, it passed along a south-eastern to a south-western direction relative to the study sites if it made landfall, or it passed along the southern coastline (Figures 1, 3 and 4; Table 1). This resulted in north-eastern to south-eastern aspects being more exposed (Figure 4). Maximum EV was lower for reconstructed hurricanes that made landfall when compared with the three most recent hurricanes that did not make landfall. The reason for this discrepancy was that maps for the three most recent hurricanes were created using actual images of each hurricane and the EV maps were therefore more accurate. If the maximum EV values from the reconstructed hurricanes were compared, the hurricanes that made landfall all had a higher maximum EV value, unless wind speed at the eye was lower than that of the eye or outer bands of other hurricanes.

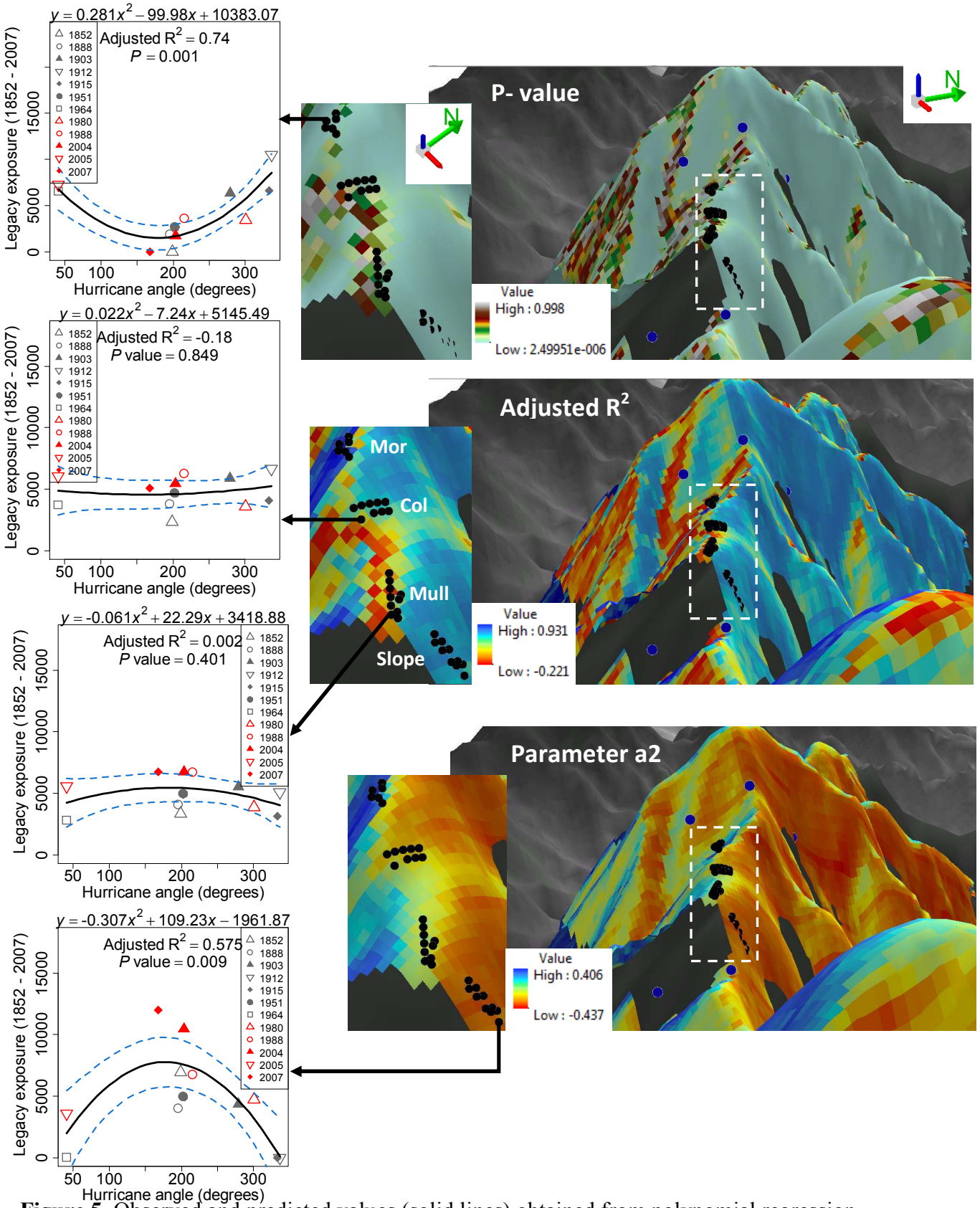

744 **Figure 5**. Observed and predicted values (solid lines) obtained from polynomial regression
745 models of the relationship between hurricane direction and a time series of exposure
746 vulnerability (for 12 hurricanes during 1852–2007 or Legacy exposure), at several of Tanner's
747 (1977) plot locations (black dots) in the Blue Mountains, Jamaica. Dashed blue lines = standard
748 error. Blue dots in the larger maps = Bellingham et al.'s (1991) plot locations.

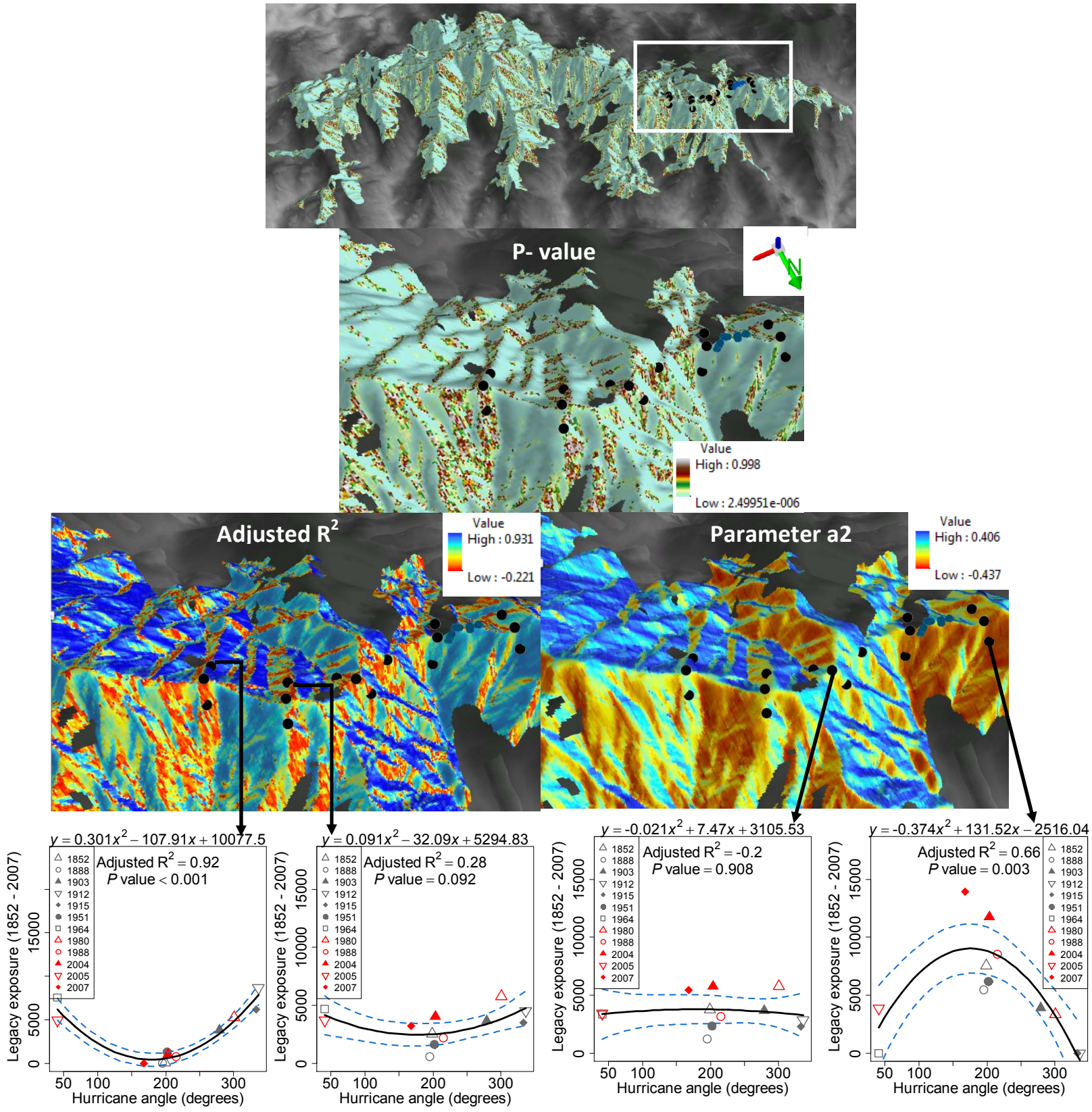

749 **Figure 6**. Observed and predicted values (solid lines) obtained from polynomial regression
750 models of the relationship between hurricane dir ection and a time series of exposure
751 vulnerability (for 12 hurricanes during 1852–2007 or Legacy exposure), at several of Bellingham
752 et al.'s (1991) plot locations (black dots) in the Blue Mountains, Jamaica. Dashed blue lines =
753 standard error.

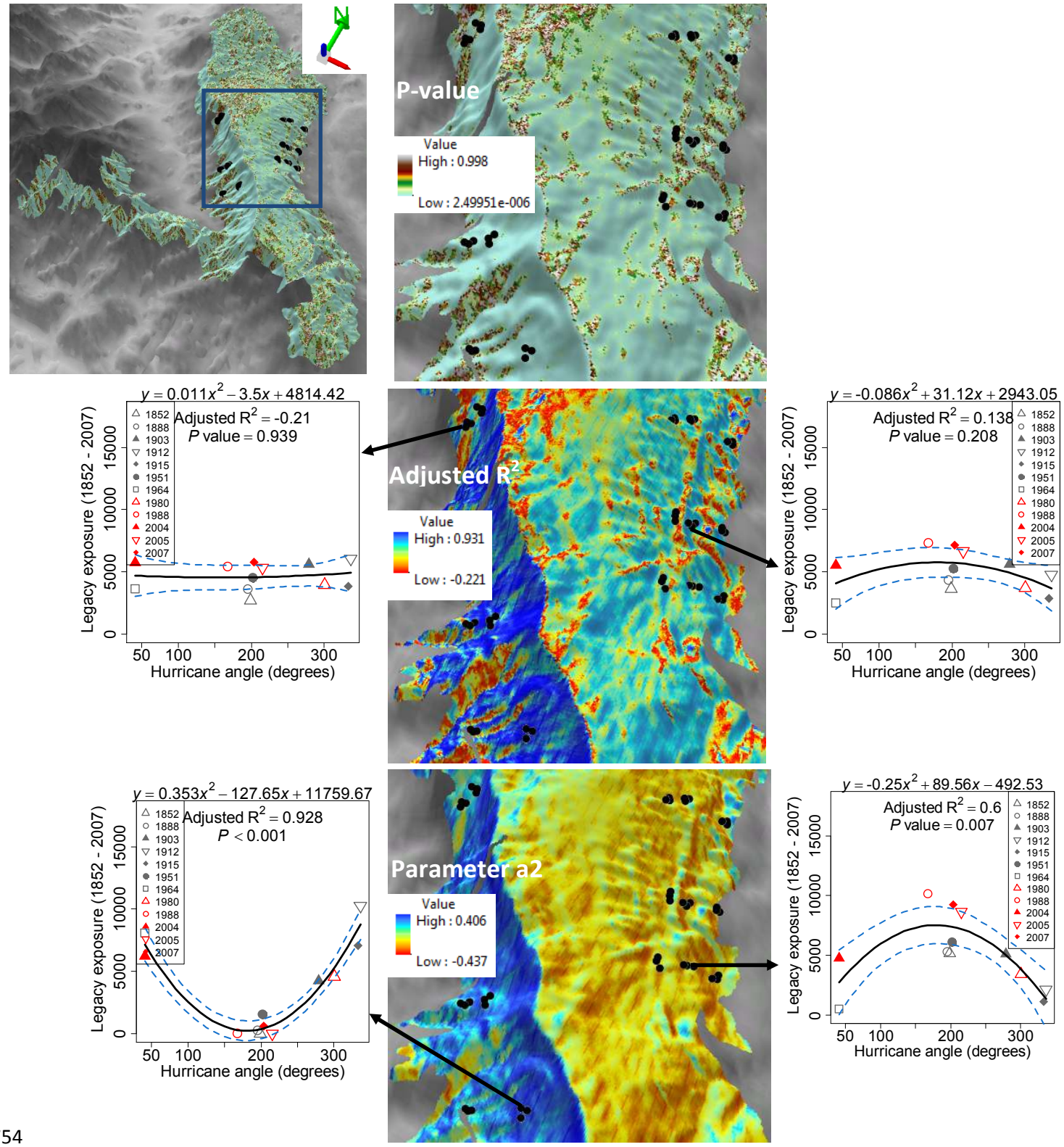

Figure 7. Observed and predicted values (solid lines) obtained from polynomial regression models of the relationship between hurricane direction and a time series of exposure vulnerability (for 12 hurricanes during 1852–2007 or Legacy exposure), at several of Luke et al.'s (2016a) plot locations (black dots) in the John Crow Mountains, Jamaica. Dashed blue lines = standard error.

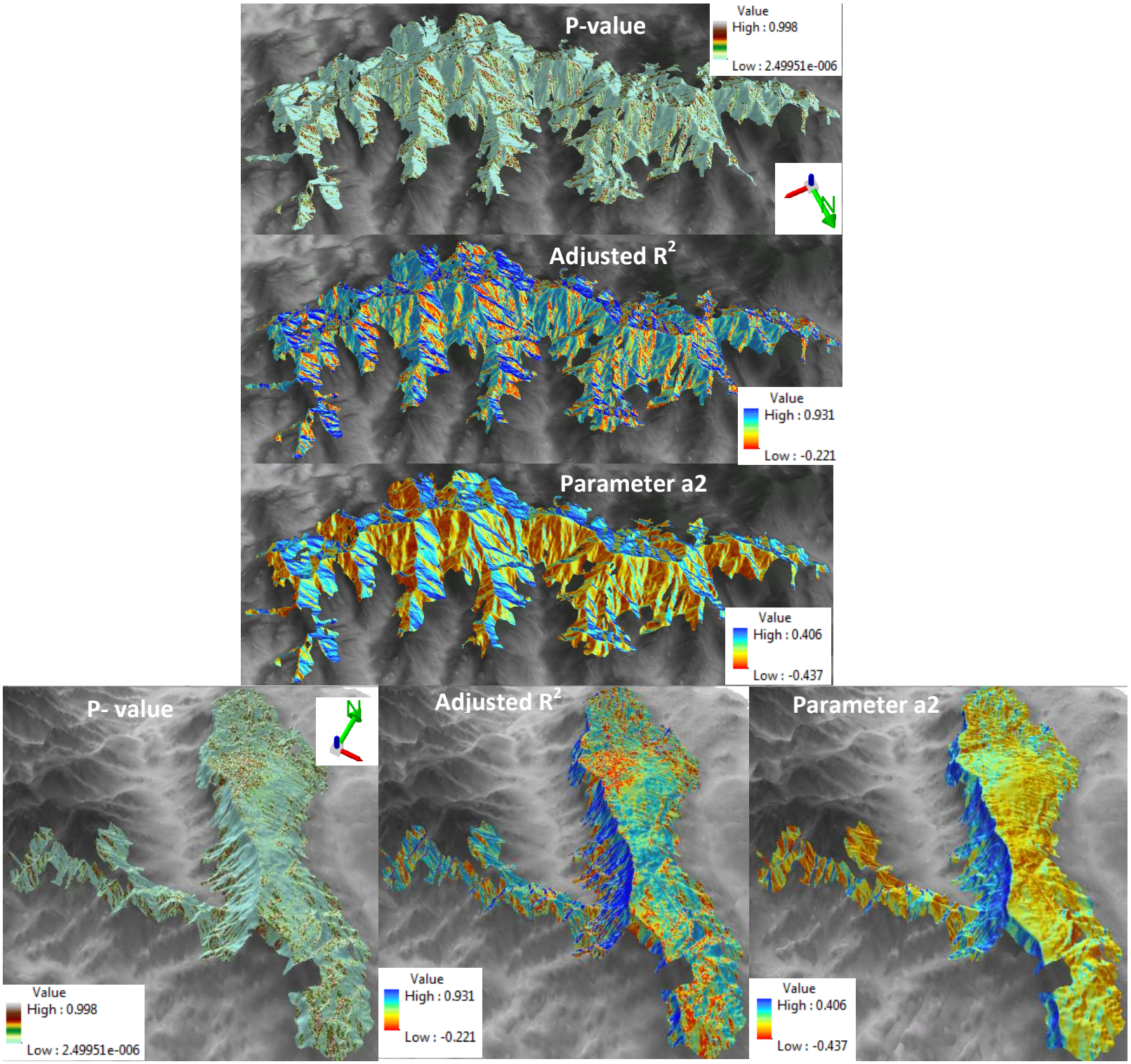

Figure 8. Three dimensional views of the outputs from the Curve Fit pixel-level polynomial regression (clipped to the undisturbed forest types in the Blue [top three] and the John Crow [bottom three] Mountains) that was used to assess the influence of average direction (in degrees) of each hurricane at its closest point (independent variable) to the coastline of Jamaica, relative to the center of the Blue and John Crow Mountains, and a time series of exposure vulnerability maps (for 12 hurricanes during 1852–2007 or Legacy exposure) for the Blue Mountains (dependent variable). Value = highest and lowest values for Curve Fit maps.

When the influences of the distance from the eye and the cardinal direction of the track of the eye on the spatial pattern of EV were considered for all hurricanes, the angle or cardinal direction of the track of the eye had a much greater influence on the spatial pattern of EV. In particular, for the Curve Fit P-value cardinal direction map, 78.5% of the pixels had a value of $P < 0.05$, whereas for the Curve Fit P-value hurricane distance map, only 7.8% of the pixels had a value of $P < 0.05$. Therefore, the distance results were not presented. Angle or cardinal direction of the tracks of the eyes of hurricanes were more important because most of the hurricanes considered in this study either made landfall or passed extremely close to the coast of Jamaica (Figure 1; Table 1). Distance affected the severity of damage caused by the winds, and hence the magnitude of the EV values, but this was dependent on the strength of the winds at the eye and at the outer bands of the hurricanes (Figures 3 and 4; Table 1). If wind speed was very high at the eye and/or at the outer bands, the EV values were usually higher (Figures 3 and 4; Table 1).

Several outputs from the Curve Fit extension can be used to explain the spatial pattern of long-term EV across the landscape and at the stand-level (Figures 5–8). For example, data extracted from the parameter a2 map can be used to separate EV based on aspect (Figures 5–8). Negative and positive parameter a2 values indicate whether the relationship between EV and the cardinal direction of the hurricane was concave or convex, respectively. This indicated that there was higher EV when the hurricanes passed to the north or south of a site, respectively (Figures 5–8). Negative (concave) and positive (convex) parameter a2 values were almost exclusively found on the northern- and southern- facing slopes, respectively, or on aspects that were more likely to be exposed when a hurricane passed to the north or south of the site, respectively (Figures 5–8). Depending on plot location and the cardinal direction of the tracks of the eyes of hurricanes,

792 three main patterns of EV can be identified at the stand-level: (1) plots that were highly exposed
793 to all hurricanes irrespective of the cardinal direction of the tracks of the eyes ($R^2 < 0.3$, and *P*-
794 value ≥ 0.05), (2) plots with an inverted U-shaped (convex) relationship that had significantly
795 higher EVs when the tracks of the eyes of the hurricanes had a southerly cardinal direction ($a2 >$
796 0), and significantly lower EVs when the of the tracks of the eyes of the hurricanes had more
797 northerly cardinal directions, or (3) plots with a U-shaped (concave) relationship that had
798 significantly lower EVs when the tracks of the eyes of the hurricanes had more southerly
799 cardinal directions ($a2 < 0$), and significantly higher EVs when the hurricanes had more
800 northerly cardinal directions (Figures 5–7).
801
802 ***Modelling stand-level tree diversity and density spatiotemporal patterns***
803 Tree Shannon diversity for the period 1974–2009, calculated from Tanner's plot data, was best
804 explained (the most parsimonious model) by average 'legacy' EV for the period 1903–1988
805 (hurricanes in 1903, 1913, 1915, 1951, 1964 and 1988) (Figure 9a; Tables 4 and 5). Hurricane
806 Allen (1980) and hurricanes that affected the site before 1903 and after 1988 were not included
807 in the calculation of legacy EV because they did not improve model fit. Shannon diversity was
808 highest at the lowest and intermediate (where it peaked) legacy EV values, but Shannon diversity
809 was much lower at the highest legacy EV values (Figure 9a). Using data from Bellingham's
810 plots, the best predictor of overall Shannon diversity patterns was the P-value output from the
811 *calc* function that encompassed 1852–1988 (Figure 9b; Tables 4 and 5). Locations with the
812 lowest P-values, particularly locations with the strongest relationship between EV and the
813 cardinal direction of the track of a hurricane's eye (which were highly exposed when the track
814 passed either to the north or the south of the sites), had the highest Shannon diversity overall;

values decreased as P-values increased and became non-significant (sites that are always exposed to hurricanes, regardless of the angle of the track of eye) (Figure 9b). There were no significant overall relationships between Shannon diversity values and the parameters that were assessed for the JCM using data from Luke et al. (2016a). However, Luke et al. (2016a) found that Shannon diversity values for the 2012 plot data increased as average EV for the three most recent hurricanes (Ivan, Dennis and Dean) increased.

Tree (stem) density, calculated using data from Tanner's plots, was overall best explained by topographic position index (result not presented here), whereas for Bellingham's plot data, the most important predictor of tree density was the adjusted R^2 values (Figures 9c; Tables 4 and 5). For the latter, tree density peaked at sites that were always exposed to hurricanes that affected the site during 1852–1988, regardless of the cardinal direction of their tracks (adjusted $R^2 = 0.2 – 0.4$). Tree density in the JCM was highest at more exposed aspects (Luke et al. 2016a). Therefore, the most important predictor of tree density was average legacy EV (1988–2007), with higher tree (stem) densities at higher EVs (Figures 9d; Tables 4 and 5). For the individual censuses of Tanner's plots, the best predictor of Shannon diversity for the census years 1974, 1984, 1989, 1991 and 1994 was average (legacy) EV for hurricanes that affected the site over the period 1903–1964 (Figures 9e–i; Table 6). For the year 2009, legacy EV for hurricanes in the period 1915–1988, was the best predictor (Figures 9j; Table 6). The individual censuses reflected the overall diversity pattern, with Shannon diversity being highest at lower and intermediate legacy EV values and lower at the highest values (Figures 9e–j). The marginal R^2 increased from 33% in 1974 to 43% in 1984, then subsequently decreased in 1989 (40.5%) until 1994 (25.6 %) (Table 6). It increased again in 2009 (31.8%). There were no important predictors of Shannon

diversity in 2004. Similarly, for Bellingham's plots, Shannon diversity in 2004 was best explained by legacy EV (hurricanes in the period 1903–1988), with the highest diversity values occurring at intermediate EV values (Figure 9k; Table 6).

Table 4. The best predictors of overall (regardless of census) tree diversity calculated as Shannon-Wiener H' and stem density calculated using data from Tanner's (ET) and Bellingham's (PJB) plots in the Blue Mountains (BM), Jamaica, and stem density from Luke et al.'s plots in the John Crow Mountain (JCM), Jamaica. Important variables included 'legacy' (average) exposure vulnerability to hurricanes during the period 1903–1988 (Exposure), Curve Fit (ET and JCM) and *calc* (PJB) outputs (P-value, Parameter a2, Adjusted R^2) and topographic parameters (Aspect).

Site	Smoother and/or distribution	Variable	Parameters	DIC	mR^2
BM (ET)	RW1	H'	Exposure	23.19	25.3
BM (ET)	RW1	H'	Parameter a2	29.36	23.2
BM (ET)	RW1	H'	Adjusted R^2	31.87	22.9
BM (ET)	RW1	H'	Aspect	34.54	22.0
BM (PJB)	Gamma	H'	P-value	22.51	32.9
BM (PJB)	RW2 Gamma	H'	Adjusted R^2 + (Adjusted R^2)^2	23.57	34.7
BM (PJB)	RW2 Gamma	H'	Exposure	31.87	30.62
BM (PJB)	RW2 Gamma	Density	Adjusted R^2	-69.2	85.1
BM (PJB)	RW2 Gamma	Density	P-value	-54.1	79.0
BM (PJB)	Gamma	Density	Exposure	-17	40.5
BM (PJB)	RW2 Gamma	Density	Aspect	-10.7	37.7
JCM	RW1 Gamma	Density	Exposure	-156.2	27.1
JCM	RW1 Gamma	Density	Parameter a2	-154.7	26.6
JCM	Gamma	Density	Aspect	-154.8	24.2
JCM	Gamma	Density	Adjusted R^2	-142.7	17.6

DIC = Deviance Information Criterion; mR^2 = marginal R-squared (%); Gamma = Gamma likelihood; RW1/RW2 = first or second-order random walk process (smoother).

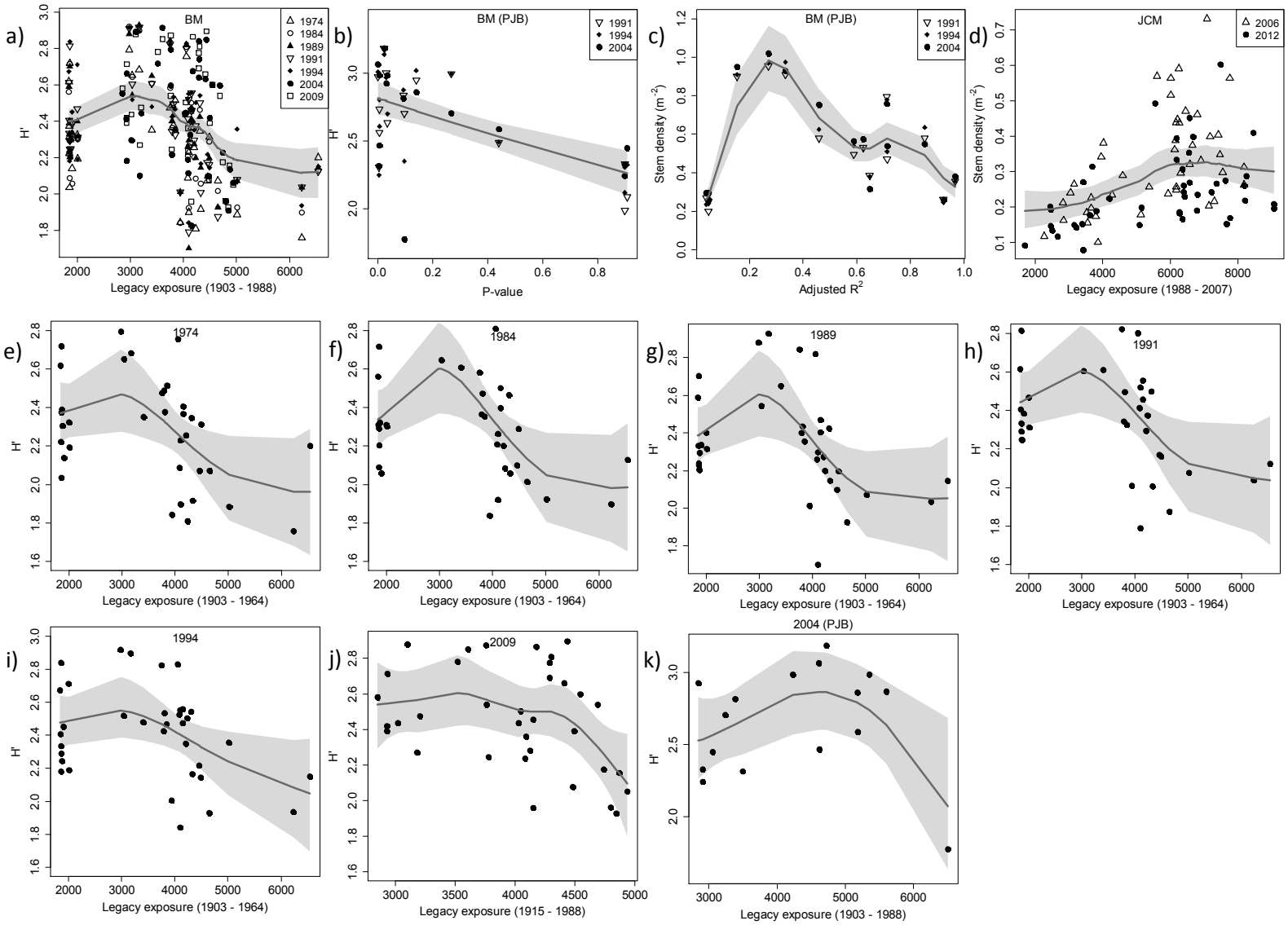

Figure 9. Observed and predicted mean values (solid lines) and the 95% Bayesian credible intervals for the posterior distribution (shade) obtained from hierarchal Bayesian space-time models for the best predictor of overall (regardless of time) a) diversity calculated as Shannon–Wiener diversity index (H') for the Blue Mountains (BM), Jamaica, using data from Tanner's plots, b) H'and c) stem density values for the BM, calculated using data from Bellingham's plots, and d) stem density values for the John Crow Mountains (JCM), Jamaica, calculated using data from Luke et al.'s plots and best predictor of H' values for each census, calculated using data from e–j) Tanner's and k) Bellingham's plots in the BM. Important variables included 'legacy' (average) exposure vulnerability for different periods/years and the *calc* output (P-Value and Adjusted R^2).

Table 5. Summary of the marginal posterior distribution for model parameters obtained from hierarchical INLA Bayesian space-time models for the best predictors of overall (regardless of census) diversity calculated as Shannon-Wiener H' and stem density calculated using data from Tanner's (ET) and Bellingham's (PJB) plots in the Blue Mountains (BM), Jamaica and stem density calculated from Luke et al.'s plots in the John Crow Mountain (JCM), Jamaica. Important variables (95% credible intervals did not contain zero) included 'legacy' average exposure vulnerability to hurricanes during the periods 1903–1988 for the ET plots and 1988–2007 for the JCM plots (Exposure) and *calc* outputs (P-value).

Site	Variable	Parameters	Mean	$Q_{0.025}$	$Q_{0.975}$	mR^2	Priors
BM (ET)	H'	Intercept	2.38	2.34	2.41	25.3	
		obs.var	0.062	0.051	0.076		
	RW1	Exposure.var	0.003	0.001	0.006		0.009, 0.05
		spde.var.nom	0.000102	-0.000015	0.000683		0.0023, 0.5
		spde.range.nom	6.0	0.5	27.9		3.9, 0.5
		AR.rho	-0.02	-0.99	0.98		
BM (PJB)	H'	Intercept	1.0	0.99	1.1	32.9	
	Gamma	P-value	-0.2	-0.3	-0.1		
		obs.var	0.01	0.009	0.02		
		spde.var.nom	0.00003	-0.0000004	0.0002		0.0023, 0.5
		spde.range.nom	4.8	0.5	19.9		3.9, 0.5
		AR.rho	0.004	-1.0	1.0		
BM (PJB)	Density	Intercept	-0.7	-0.7	-0.6	85.1	
	Gamma	obs.var	0.04	0.03	0.07		
	RW2	Adjusted R^2.var	0.09	0.04	0.17		0.065, 0.05
		spde.var.nom	0.00002	-0.0000003	0.0001		0.0023, 0.5
		spde.range.nom	7.9	0.7	40.1		3.9, 0.5
		AR.rho	0.002	-1.0	1.0		
JCM	Density	Intercept	-1.30	-1.37	-1.22	27.1	
	Gamma	obs.var	0.14	0.10	0.19		
	RW1	Exposure.var	0.009	0.003	0.021		0.03, 0.05
		spde.var.nom	0.0000232	-0.0000009	0.0001545		0.002, 0.5
		spde.range.nom	6.4	0.7	29.9		4, 0.5
		AR.rho	-0.002	-0.988	0.988		

$Q_{0.025}$ and $Q_{0.975}$ = quantiles of the credible interval; DIC = Deviance Information Criterion; mR^2 = marginal R-squared (%);Gamma = Gamma likelihood; RW1/RW2 = first or second-order random walk process (predictor variance is followed by .var, e.g., Exposure.var for RW1 and Prior = reference standard deviation and the right tail probability); obs.var = model variance; spde.var.nom = nominal spatial variance (Priors = prior marginal standard deviation and right tail probability); spde.range.nom = nominal spatial range (km) (Priors = practical range and right tail probability); AR.rho = autoregressive parameter, temporal correlation coefficient.

Table 6. Summary of the marginal posterior distribution for model parameters obtained from hierarchical INLA Bayesian space-time models for the best predictors of diversity calculated as Shannon-Wiener H-Index from Tanner's (ET) and Bellingham's (PB) plots in the Blue Mountains, Jamaica, for each census. Average exposure vulnerability (Expos) to hurricanes during the period 1903–1988 was the most important variable (95% credible intervals did not contain zero).

Site	Variable	Parameters	Mean	$Q_{0.025}$	$Q_{0.975}$	mR^2	Priors
BM	H'	Intercept	2.28	2.20	2.37	33	
ET	1974	obs.var	0.06	0.03	0.10		
	RW2	Expos (1903 -1964).var	0.0732	0.0005	0.3326		0.3, 0.05
		spde.var.nom	0.0000234	-0.0000003	0.0001544		0.0023, 0.5
		spde.range.nom	7.3	0.7	35.6		3.9, 0.5
BM	H'	Intercept	2.32	2.24	2.40	43	
ET	1984	obs.var	0.05	0.03	0.08		
	RW2	Expos (1903 -1964).var	0.114	0.010	0.380		0.3, 0.05
		spde.var.nom	0.0000194	-0.0000004	0.0001249		0.0023, 0.5
		spde.range.nom	8.1	0.7	40.8		3.9, 0.5
BM	H'	Intercept	2.35	2.27	2.43	40.5	
ET	1989	obs.var	0.05	0.03	0.08		
	RW2	Expos (1903 -1964).var	0.101	0.007	0.345		0.3, 0.05
		spde.var.nom	0.0000183	-0.0000004	0.0001159		0.0023, 0.5
		spde.range.nom	7.9	0.7	39.7		3.9, 0.5
BM	H'	Intercept	2.38	2.30	2.46	37.9	
ET	1991	obs.var	0.05	0.03	0.09		
	RW2	Expos (1903 -1964).var	0.0749	0.0023	0.2896		0.3, 0.05
		spde.var.nom	0.0000181	-0.0000004	0.0001139		0.0023, 0.5
		spde.range.nom	8.2	0.8	41.8		3.9, 0.5
BM	H'	Intercept	2.41	2.33	2.50	25.6	
ET	1994	obs.var	0.06	0.04	0.10		
	RW2	Expos (1903 -1964).var	0.0479	0.0003	0.4525		0.3, 0.05
		spde.var.nom	0.0000192	-0.0000004	0.0001230		0.0023, 0.5
		spde.range.nom	8.1	0.7	41.0		3.9, 0.5
BM	H'	Intercept	2.46	2.38	2.55	31.8	
ET	2009	obs.var	0.06	0.04	0.10		
	RW2	Expos (1915 -1988).var	0.0414	0.0002	0.4477		0.3, 0.05
		spde.var.nom	0.0000300	-0.0000005	0.0002044		0.0023, 0.5
		spde.range.nom	5.1	0.6	21.9		3.9, 0.5
BM	H'	Intercept	0.98	0.92	1.04	51.1	
PB	2009	obs.var	0.013	0.006	0.027		
	RW2	Expos (1903 -1988).var	0.0024	0.0003	0.0083		0.05, 0.05
		spde.var.nom	0.0000185	-0.0000004	0.0001167		0.0023, 0.5
		spde.range.nom	8.2	0.8	41.3		3.9, 0.5

$Q_{0.025}$ and $Q_{0.975}$ = quantiles of the credible interval; mR^2 = marginal R-squared (%); RW2 = random second-order random walk process (predictor variance is followed by .var, e.g., Expos.var for RW2 and Prior = reference standard deviation and the right tail probability); Gamma = Gamma likelihood; obs.var = model variance; spde.var.nom = nominal spatial variance (Priors = prior marginal standard deviation

and right tail probability); spde.range.nom = nominal spatial range (km) (Priors = practical range and right tail probability); AR.rho = autoregressive parameter, temporal correlation coefficient.

Discussion

Topographic exposure in the Blue and John Crow Mountains

Topographic exposure models are generally used to identify points on a landscape-scale topographic surface that are protected from (wind shadow) or exposed to specific wind directions (Boose et al. 1994). The wind shadow is estimated by assuming that the wind bends downwards at a fixed inflection angle from the horizontal as it passes over an elevated surface (Boose et al. 1994). It does not however, estimate changes in wind speed or direction caused by local topography (Boose et al. 1994). In addition, exposure models do not consider the movement of wind over complex terrain and meteorological conditions usually found near the center of a hurricane such as steep gradients of pressure velocity, local convective cells and curved wind paths and rain bands (Boose et al. 1994). Also, exposure models do not consider changes or alterations in these gradients at fixed locations due to a storm's forward movement, intensification or weakening (Boose et al. 1994). These complexities are difficult and problematic to model (Boose et al. 1994).

The simple topographic exposure model used in our study therefore lacks complexity, nevertheless, exposure models work at landscape scales (≈ 10 km) and provide useful predictions of areas protected from or exposed to damaging winds (Boose et al.1994). Also, reconstructed landscape-level exposure maps are generally tested by comparing predicted exposure to actual landscape-level (Boose et al. 1994) or stand-level damage (e.g. Batke et al. 2014; Negrón-Juárez et al. 2014a and 2014b; Luke et al. 2016a) to determine if they can be used as proxies for

929 hurricane damage. Stand-level damage data are generally collected within 2 years within after a
930 disturbance event, although stand-level damage data have been collected up to 12 years after a
931 hurricane stuck (Gannon and Martin 2014). In our study, the reconstructed exposure maps for
932 Hurricane Gilbert were tested or evaluated using stand-level damage and recovery data from
933 Bellingham's plots, which were collected 20–23 months after that hurricane struck the BM.
934 Bellingham's plots included locations with a wider range of topographic positions (Bellingham
935 and Tanner 2000) (Figure 7) and were more suitable for the EV model evaluation than those of
936 Tanner. Tanner's plots varied more in topographic position than in EV due to the location of the
937 plots in nearby blocks located in strongly contrasting topographic positions (Figure 7). As such,
938 Bellingham's plot data showed a stronger relationship of damage and recovery to EV and have
939 greater general validity/power for this analysis than do Tanner's plot data (Figure 2; Tables 2 and
940 3). The method presented in this study can therefore be used to reconstruct past hurricane
941 (legacy) EV, which can be used as a proxy for landscape-scale hurricane disturbance/damage at
942 un-sampled locations and for hurricanes for which no disturbance data are available. We found
943 that if less ideal proxies were used, at the very least they could be used to produce landscape-
944 level maps that summarize the extent of forest recovery.
945
946 At the landscape scale, the spatial pattern of hurricane exposure that was reported in this study
947 was consistent other published observations. In the southern hemisphere, disturbance severity is
948 usually greater on the left side of a cyclone's path due to clockwise rotation of cyclone winds.
949 For example, large areas of undisturbed forest were found on the right side of the track of
950 tropical cyclone Yasi after it struck the northeastern rainforests of Queensland, Australia
951 (Negrón-Juárez et al. 2014a and 2014b). In contrast, in the northern hemisphere (US Gulf Coast

forest ecosystems), forest disturbance severity was observed to be greater on the right side of the tracks of four hurricanes (Negrón-Juárez et al. 2014a) due to counter-clockwise rotation of cyclone winds. Additionally, in central new England, USA, the most destructive winds of a 1938 hurricane occurred to the east (right) of the eye where the highest wind speeds were produced from the anticlockwise rotary velocity and forward movement (Foster, 1988). In addition, damage was lower to the west (left) of the eye where wind speeds were lower (Foster, 1988). These observations were consistent with those of Boose et al. (1994), who found that as Hurricane Hugo approached the Luquillo Experiment Forest (LEF), Puerto Rico, from the east, with a track that was initially oriented to the south of the site, the strongest winds associated with the leading eye wall were to the northeast (to the right). At the same site, after ≈ 2 hrs, the trailing eyewall winds were weaker and were from the SSW (Boose et al. 1994). As a result, the north-facing slopes of the LEF were more exposed and the southern slopes, facing the weaker trailing eyewall winds from the SW and SSW, were less exposed (Boose et al. 1994) and showed little damage (Scatena and Larsen 1991). Similarly, after tropical cyclone Yasi struck the northeastern rainforests of Queensland, forest disturbance was found to be higher at aspects that were facing away from the dominant surface winds (Negrón-Juárez et al. 2014b).

In our study, the orientation of the tracks of the eye or center of the hurricanes, even if they made landfall, passed either to the north or south of the study sites and this influenced the pattern of exposure (Figures 4–8). We found that when the eye of a hurricane followed a path or track with a southern orientation, the pattern of exposure was similar to other reported observations; that is, the right side of the track (the north-eastern to south-eastern aspects) were more exposed (Figures 4–8). However, when the eye followed a northern orientation, wind bands from the

975 leading eye wall were mostly offshore, and it was the wind bands from the trailing eye wall that
976 passed over the sites, resulting in greater exposure on the left side of the track (the southern to
977 south-western aspects) (Figures 4–8). Furthermore, there were equal numbers of hurricanes (six
978 each) that followed a path north or south of the sites, and multiple hurricanes followed a similar
979 path in relatively quick succession (Figures 1, 3 and 4). For example, two hurricanes, in 1852
980 and 1889, had tracks to the south of Jamaica and three hurricanes that made landfall over a
981 period of 12 years (1903, 1912 and 1915) had northerly tracks (Figures 1, 3 and 4). Also, four
982 hurricanes made landfall over a period of 48 years (1903–1951) or followed a track to the north
983 of the island in 61 years (1903–1964) (Figures 1, 3 and 4). Since 1988, most hurricanes followed
984 a track to the south (four in 19 years), although only one made landfall (Gilbert) (Figures 1, 3
985 and 4). Therefore, since 1852, most aspects at the two sites have been exposed to multiple
986 hurricanes, with only locations with a north-western aspect being severely exposed to only a
987 single hurricane (Allen in 1980) (Figure 4). At the two study sites (both on steeply-sloped
988 mountain ranges), exposure, hence disturbance history at the stand- level, was a function of angle
989 or cardinal direction of both hurricane tracks and local topography (Figures 5–8). As a result, the
990 stand-level assessments of hurricane impacts in the BM and JCM were strongly influenced by
991 plot location. Some plots, despite being located close to each other, had a different disturbance
992 history or degree of exposure (Bellingham et al. 1991), while the disturbance history and
993 exposure was similar for some plots that were located far away from each other (Figures 5–7).
994
995 ***The impact of legacy hurricanes on stand-level spatiotemporal diversity and density patterns***
996 Advances in historical hurricane damage modelling create opportunities for improving estimates
997 of hurricane impacts (Logan and Xu 2015). Models can now account for temporal correlation

998 and spatial dependence simultaneously (Logan and Xu 2015). Therefore, these models can be
999 used (and were used in this study to evaluate 1) whether individual hurricanes had effects, 2)
1000 whether it was only the most severe hurricanes that made a difference, 3) whether it was the
1001 cumulative effect of several hurricanes over many years that was more important and 4) whether
1002 the hurricane effects were temporary or prolonged (Logan and Xu 2015). For the BM, there was
1003 an increase in tree diversity at the stand-level in the decades following the passage of Hurricane
1004 Gilbert (Tanner and Bellingham 2006). However, diversity also increased during the pre-Gilbert
1005 census period and there were mostly light-demanding species present in the canopy in 1974
1006 (Tanner and Bellingham 2006), possibly due to the effects of previous disturbances, including
1007 hurricanes. Also, five hurricanes struck in 61 years (1903–1964), four of which made landfall
1008 over a period of 48 years (1903–1951), and the eyes or centers of four hurricanes followed a
1009 more northerly track (Figures 1, 3 and 4). The BM were therefore exposed to frequent high-
1010 intensity hurricanes and, as such, the heterogeneity of disturbance caused by, for example, the
1011 1903 hurricane may have been maintained for an extended period (85 years) by successive
1012 hurricanes (Figure 4). This may have permitted greater species co-existence at sites with
1013 intermediate exposure and an increase in diversity to occur over time, even after Hurricane
1014 Gilbert affected the BM. As a result, the influence of legacy EV on the pattern of diversity, that
1015 is peak diversity at intermediate exposures, was similar overall (regardless of time) (Figure 9a)
1016 and for the individual censuses of both Tanner's and Bellingham's plots (Figures 9e–k). This is
1017 despite the two sets of plots differing in the number, size, shape and layout or design. However,
1018 for Bellingham's plots, the effects of past disturbance were manifest in a different way. In
1019 particular, the magnitude of exposure resulting from the cardinal direction or orientation of the
1020 hurricane's eye or center (P-value from the *calc* function) was the most important predictor of

1021 tree Shannon diversity and density in Bellingham's plots (Figure 9b). That is, tree diversity was
1022 highest at plot locations that were more likely to be exposed when a hurricane's eye followed a
1023 track that was either to the north or to the south of the sites, and lowest at sites that were highly
1024 exposed to all hurricanes . In contrast, tree density peaked at sites that were always exposed,
1025 regardless of the cardinal direction of the center of the hurricanes (Figure 9c). Both patterns, with
1026 that for diversity also being found for the clustered Tanner plots, agree with the two hypotheses,
1027 i.e. tree diversity was highest at sites subject to intermediate levels of disturbance but tree density
1028 was greatest at sites subject to the highest levels of disturbance. Differences between the two
1029 data sets in terms of the importance of predictors of exposure may be due to plot location.
1030 Tanner's plots were purposefully located in four clusters each placed in a contrasting forest type
1031 that occurred in close proximity (Tanner 1977), whereas Bellingham's plots were located in a
1032 more dispersed sampling design stratified between three topographic positions (Bellingham
1033 1991) (Figures 5 and 6).
1034
1035 The results from the individual census assessments can be used to determine when the effects of
1036 a hurricane on tree diversity and density became important or for how long their effects lasted.
1037 Average legacy exposure of five hurricanes occurring during 1903–1964 was the most important
1038 predictor of diversity in Tanner's plots in 1974, and this effect lasted until 1994 or 91 years
1039 (Figures 9e–i). Exposure vulnerability to Hurricane Gilbert was not important in these plots
1040 (because it did not improve model fit) until 21 years after the hurricane affected the plots (Figure
1041 9j). For Bellingham's plots, average 1903–1988 legacy exposure, which included the EV for
1042 Hurricane Gilbert, was important in 2004, 16 years after Gilbert struck, and the 1903 hurricane
1043 was still important 101 years after it struck (Figure 9k). In comparison, the effects of three

1044 successive hurricanes that made landfall (in 1928, 1931 and 1932) on forest structure and
1045 composition in the Luquillo Experimental Forest, Puerto Rico, lasted for nearly 50 years after the
1046 last hurricane (Weaver 2002). Moreover, stand-level spatiotemporal patterns in tree diversity in
1047 the BM plots are likely to have been most influenced by the hurricanes that made landfall, with
1048 their highest wind speeds closest to the study sites. With the exception of Hurricane Cleo in
1049 1964, all other hurricanes that passed Jamaica at some distance off the coast had little or no
1050 influence.
1051
1052 Although the BM and JCM had a similar disturbance history, the effects of hurricane disturbance
1053 were manifest in different ways. In particular, we found that forest type influenced the
1054 heterogeneity of forest damage across a landscape (Zimmerman et al. 1994; Everham and
1055 Brokaw 1996; Boose et al. 2004).The ridge-top forest of the BM was found to be the least
1056 damaged (the least crown breakage and little tree uprooting) of four Jamaican forests that were
1057 assessed 3–8 months following the passage of Hurricane Gilbert (Bellingham et al. 1992). This
1058 was attributed to greater resistance of the ridge-top forest to winds, due to a more streamlined,
1059 aerodynamic and even canopy, because of its exposed topographic position (Bellingham et al.
1060 1992). Also, there had presumably been a strong selection for tree species and/or structural
1061 characteristics (shorter canopy and greater ratio of stem width to height (Lawton 1982)) with
1062 greater resistance to strong winds (Bellingham et al. 1992). In contrast, trees in the lower
1063 montane forest of the JCM were found to be more susceptible to uprooting than at the other sites
1064 due to the greater impact of Hurricane Gilbert on this site, the greater average height of trees, and
1065 poor anchoring of trees due to the limestone substrate (Bellingham et al. 1992). The JCM may
1066 have also been more affected than the BM by the outer bands of the last three hurricanes that

1067 passed 40–45 km from the island (Figures 3 and 4). There were obvious signs of hurricane
1068 damage in the JCM after Hurricanes Ivan and Dennis struck (pers. obs.), and eight months after
1069 Hurricane Dean, in 2004, 2005 and 2007, respectively (Luke et al. 2016a), but no obvious
1070 evidence of damage or disturbance was found in the BM plots during the 2009 census (Tanner et
1071 al. 2014). As a result, EV from these hurricanes was not an important predictor of spatial
1072 variation in tree density and/or diversity in the BM (or the effects take longer to become
1073 manifest). Individual hurricane EV, or the average EV for the last three hurricanes, was however
1074 an important predictor of stand-level data from the JCM, in particular individual tree and
1075 community structural changes in 2012, diversity patterns in 2012, and density patterns in 2006
1076 and 2016 (Luke et al. 2016a), and across both censuses of the plots (2006 and 2012). However,
1077 individual hurricane EV or the average over past hurricanes could not be used to explain the
1078 2006 stand-level diversity patterns. Species composition of the JCM plots may have either
1079 recovered by 2006, after the JCM was struck by Hurricane Gilbert in 1988, or the impact of
1080 Hurricanes Ivan and Dennis may have masked the effects of Gilbert and other past hurricanes.
1081
1082 The rate of turnover of tree stems and species is another potential explanation for the differences
1083 between the BM and JCM. Low turnover rates can be equated to greater resistance to hurricane
1084 damage (Tanner and Bellingham 2006). After Hurricane Gilbert, turnover of tree stems for the
1085 period 1990–1994 was 2.6% yr^{-1} for Bellingham's plot data (Bellingham and Tanner 2000), and
1086 4.06% yr^{-1} for the period 1989–1994 and 1.6% yr^{-1} for the period 2004–2009 for Tanner's plot
1087 data (Tanner and Bellingham 2006). In comparison, over the period 2006–2012, turnover was
1088 2.9% yr^{-1}, for trees in the JCM following Hurricanes Ivan, Dennis and Dean (Luke et al.
1089 2016a,b). As such, turnover at the stand-level for the JCM was within the range of values for the

1090 BM after Gilbert made landfall, but higher than the BM during a period that overlapped, when
1091 three hurricanes passed closed to the island. Additionally, 25–50% of trees 2–10 cm in DBH died
1092 during the period 2006–2012 in the JCM (Luke et al. 2016b), likely removing some of the trees
1093 recruited since Hurricane Gilbert (and before). Moreover, in the BM, the mortality of damaged
1094 trees was 2–8 times higher than undamaged stems 19 years after Gilbert (Tanner et al. 2014).
1095 Therefore, the greater resistance and recovery of trees in the BM may have resulted in a delayed
1096 response that was manifest over a longer time. As such, the influence of Gilbert was not evident
1097 until 2004 and 2009 for tree diversity in Bellingham's and Tanner's plots, respectively, and the
1098 influence of several hurricanes was evident for long periods. In contrast, rapid changes in the
1099 JCM due to the impacts of the rapid succession of hurricanes during 2004–2007 may have
1100 removed any signs of the influence of past hurricanes. The rate of turnover of tree stems and
1101 species at the two sites were different and therefore, the effects of hurricane disturbance were
1102 manifest in different ways.
1103

1104 **Conclusion**

1105 We developed and validated a method to reconstruct and map landscape scale (≈ 10 km^2)
1106 exposure to 12 high-intensity hurricanes (category 2–4), which affected the forests of the BM
1107 and JCM in Jamaica, over the past 155 years. The maps were then aggregated and used to
1108 identify the spatial patterns of hurricane exposure and to determine if exposure could be used to
1109 explain current stand-level (≈ 1 km^2) tree diversity and density patterns. Exposure variability at
1110 the landscape and local scales was best explained by the orientation or angle of the eye or center
1111 of the hurricane relative to the coastline of Jamaica. This was used to identify three patterns of
1112 historical exposure: exposure was significantly higher to the south or north of a hurricane's track

when the track was to the north or south of the island/sites, respectively. In the BM, the pattern of exposure determined by the cardinal direction of all hurricane tracks or exposure to six hurricanes (over the period 1903–1988), five of which made landfall, was the best predictor of stand-level spatiotemporal patterns of diversity and density. In particular, there was co-existence of a greater number of species at sites with intermediate exposure (sensu the intermediate disturbance hypothesis) and the highest densities were found at sites that were always highly exposed. In the JCM, stand-level spatiotemporal variation in overall tree density (highest where exposure was highest) was explained by four of the most recent hurricanes, three of which did not make landfall. The difference in predictors between the two sites can be explained by forest type. The ridge top forest in the BM had a greater resistance to hurricane effects, as tree diversity and density were only influenced by the hurricanes that made landfall. The forest of the JCM had a lower resistance and, as such, the influence of past hurricanes was reduced by the impact of three or four of the most recent hurricanes, due to a high turnover of stems and species in the JCM over a short period of time. The reconstructed landscape-scale maps can therefore be used to provide valuable insights into the effects of past hurricanes on contemporary patterns of tree diversity and density at the stand-level (≈ 1 km^2) in different forest types.

Acknowledgements

We thank Ms Rochelle Hollingsworth and Ms Rose-Marie Rochester from Mico University College, Jamaica, who assisted with generating the exposure maps during their field-based work-experience tenure (Industry Based Component of the Practicum for their BSc degrees) and their advisor Dr Lisa Caleb, who organized their programme. In addition, Drs Haakon Bakka and James Gibbons provided statistical advice.

References

Banerjee, S., A. E. Gelfand, A. O. Finley, and H. Sang. 2008. Gaussian predictive process models for large spatial data sets. Journal of the Royal Statistical Society: Series B (Statistical Methodology) 70: 825–848.

Batke, S. P., M. Jocque, and D. L. Kelly. 2014. Modelling hurricane exposure and wind speed on a mesoclimate scale: a case study from Cusuco NP, Honduras. PloS One 9: e91306.

Bellingham, P. J. 1991. Landforms influence patterns of hurricane damage: evidence from Jamaican montane forests. Biotropica 23: 427–433.

Bellingham, P. J. 2008. Cyclone effects on Australian rain forests: An overview. Austral Ecology 33: 580–584.

Bellingham, P. J., and E. V. J. Tanner. 2000. The influence of topography on tree growth, mortality, and recruitment in a tropical montane forest. Biotropica 32: 378–384.

Bellingham, P. J., E. V. J. Tanner, and J. R. Healey. 1995. Damage and responsiveness of Jamaican montane tree species after disturbance by a hurricane. Ecology 76: 2562–2580.

1157 Bellingham, P. J., V. Kapos, N. Varty, J. R. Healey, E. V. J. Tanner, D. L. Kelly, J. W. Dalling,
1158 L. S. Burns, D. Lee, and G. Sidrak. 1992. Hurricanes need not cause high mortality: the effects
1159 of Hurricane Gilbert on forests in Jamaica. Journal of Tropical Ecology 8: 217–223
1160
1161 Bender, M. A., T. R. Knutson, R. E. Tuleya, J. J. Sirutis, G. A. Vecchi, S. T. Garner, and I. M.
1162 Held. 2010. Modeled impact of anthropogenic warming on the frequency of intense Atlantic
1163 hurricanes. Science 327: 454–458.
1164
1165 Blangiardo, M., and M. Cameletti. 2015. Spatial and spatio-temporal Bayesian models with R-
1166 INLA. John Wiley & Sons.
1167
1168 Boose, E. R., D. R. Foster, and M. Fluet. 1994. Hurricane impacts to tropical and temperate
1169 forest landscapes. Ecological Monographs 64: 369–400.
1170
1171 Boose, E. R., M. I. Serrano, and D. R. Foster. 2004. Landscape and regional impacts of
1172 hurricanes in Puerto Rico. Ecological Monographs 74: 335–352.
1173
1174 Cameletti, M., F. Lindgren, D. Simpson, and H. Rue. 2013. Spatio-temporal modeling of
1175 particulate matter concentration through the SPDE approach. AStA Advances in Statistical
1176 Analysis 97: 109–131.
1177
1178 Carslaw, D. C. and K. Ropkins. 2012. openair --- an R package for air quality data analysis.
1179 Environmental Modelling & Software 27–28: 52–61.

Chai, S. L., J. R. Healey, and E. V. J. Tanner. 2012. Evaluation of forest recovery over time and space using permanent plots monitored over 30 years in a Jamaican montane rain forest. PLoS One 7: e48859.

Connell, J. H. 1978. Diversity in tropical rain forests and coral reefs. Science 199: 1302–1310.

Cosandey-Godin, A., E. T. Krainski, B. Worm, and J. M. Flemming. 2014. Applying Bayesian spatiotemporal models to fisheries bycatch in the Canadian Arctic. Canadian Journal of Fisheries and Aquatic Sciences 72: 186–197.

Crawley, M. J. 2012. The R book. John Wiley & Sons.

Dawid, A. P. 1984. Present position and potential developments: Some personal views: Statistical theory: The prequential approach. Journal of the Royal Statistical Society. Series A (General) 147: 278–292.

De Jager, N. R., and T. J. Fox. 2013. Curve Fit: a pixel-level raster regression tool for mapping spatial patterns. Methods in Ecology and Evolution 4: 789–792.

Denslow, J. S. 1995. Disturbance and diversity in tropical rain forests: the density effect. Ecological Applications 5: 962–968.

1203 Early, D. S., and D. G. Long. 2001. Image reconstruction and enhanced resolution imaging from
1204 irregular samples. IEEE Transactions on Geoscience and Remote Sensing 39: 291–302.
1205
1206 Elsner, J. B., J. P Kossin, and T. H. Jagger. 2008. The increasing intensity of the strongest
1207 tropical cyclones. Nature 455: 92–95.
1208
1209 Everham, E. M., III, and N. V. L. Brokaw. 1996. Forest damage and recovery from catastrophic
1210 wind. Botanical Review 62: 113–185.
1211
1212 Foster, D. R. 1988. Species and stand response to catastrophic wind in central New England,
1213 USA. Journal of Ecology 76: 135-151.
1214
1215 Fuglstad, G., D. Simpson, F. Lindgren, and H. Rue. 2017. Constructing priors that penalize the
1216 complexity of gaussian random fields , pp. 1–33, arXiv.org,http://arxiv.org/abs/1503.00256.
1217
1218 Gannon, B. M., and P. H. Martin. 2014. Reconstructing hurricane disturbance in a tropical
1219 montane forest landscape in the Cordillera Central, Dominican Republic: implications for
1220 vegetation patterns and dynamics. Arctic, Antarctic, and Alpine Research 46: 767–776.
1221
1222 Gelman, A. 2005. Analysis of variance: why it is more important than ever. Annals of Statistics
1223 33: 1–31.
1224

1225 Gneiting, T., F. Balabdaoui, and A. E. Raftery. 2007. Probabilistic forecasts, calibration and
1226 sharpness. Journal of the Royal Statistical Society: Series B (Statistical Methodology) 69: 243–
1227 268.
1228
1229 Heartsill Scalley, T. 2017. Insights on forest structure and composition from long-term research
1230 in the Luquillo Mountains. Forests 8: 204.
1231
1232 Held, L., B. Schrödle, and H. Rue. 2010. Posterior and cross-validatory predictive checks: a
1233 comparison of MCMC and INLA. Pages 91-110 in Statistical modelling and regression
1234 structures. Physica-Verlag HD.
1235
1236 Hogan, J. A., J. K. Zimmerman, J. Thompson, M. Uriarte, N. G. Swenson, R. Condit, S. Hubbell,
1237 D. J. Johnson, I F. Sun, C.-H. Chang-Yang, S.-H. Su, P. Ong, L. Rodriguez, C. C. Monoy, S.
1238 Yap, and S. J. Davies 2018. The frequency of cyclonic wind storms shapes tropical forest
1239 dynamism and functional trait dispersion. Forests 9: 404.
1240
1241 Ibanez, T., G. Keppel, C. Menkes, T. W. Gillespie, M. Lengaigne, M. Mangeas, G. Rivas-Torres,
1242 and P. Birnbaum. 2019. Globally consistent impact of tropical cyclones on the structure of
1243 tropical and subtropical forests. Journal of Ecology 107: 279–292.
1244
1245 Jenness, J., B. Brost, and P. Beier. 2013. Land facet corridor designer: Topographic position
1246 index tools. Available at: http://corridordesign.org/downloads.
1247

1248 Knutson T. R., J. L. McBride, J. Chan, K. Emanuel, G. Holland, C. Landsea, I. Held, J. P.
1249 Kossin, A. K. Srivastava, and M. Sugi. 2010. Tropical cyclones and climate change. Nature
1250 Geoscience 3: 157
1251
1252 Krainski, E. T., F. Lindgren, D. Simpson, and H. Rue. 2017. The R-INLA tutorial on SPDE
1253 models. Journal of Geographical Systems. http://www. math. ntnu. no/inla/r-inla.
1254 org/tutorials/spde/spde-tutorial. pdf.
1255
1256 Lawton, R.O. 1982. Wind stress and elfin stature in a montane rain forest tree: an adaptive
1257 explanation. American Journal of Botany 69:1224–1230.
1258
1259 Lin, K. C., S. P. Hamburg, L. Wang, C. T. Duh, C. M. Huang, C. T. Chang, and T. C. Lin. 2017.
1260 Impacts of increasing typhoons on the structure and function of a subtropical forest: reflections
1261 of a changing climate. Scientific Reports 7: 4911.
1262
1263 Lindgren, F., and H. Rue. 2015. Bayesian spatial modelling with R-INLA. Journal of Statistical
1264 Software 63: 19.
1265
1266 Lindgren, F., H. Rue, and J. Lindstromm. 2011. An explicit link between Gaussian fields and
1267 Gaussian Markov random fields: The SPDE approach. Journal of the Royal Statistical Society
1268 Series B 73: 423–498.
1269

1270 Logan, J. R., and Z. Xu. 2015. Vulnerability to hurricane damage on the US Gulf Coast since
1271 1950. Geographical Review 105: 133–155.
1272
1273 Luke, D., K. McLaren, and B. Wilson. 2016a. Modeling hurricane exposure in a Caribbean lower
1274 montane tropical wet forest: The effects of frequent, intermediate disturbances and topography
1275 on forest structural dynamics and composition. Ecosystems 19: 1178–1195.
1276
1277 Luke, D., K. McLaren, and B. Wilson. 2016b. Short-term dynamics and the effects of biotic and
1278 abiotic factors on plant physiognomic groups in a hurricane-affected lower montane tropical
1279 forest. Biotropica 48: 332–341.
1280
1281 Martins, T. G., D. Simpson, F. Lindgren, and H. Rue. 2013. Bayesian computing with INLA:
1282 new features. Computational Statistics & Data Analysis 67: 68–83.
1283
1284 McGroddy, M., D. Lawrence, L. Schneider, J. Rogan, I. Zager, and B. Schmook. 2013. Damage
1285 patterns after Hurricane Dean in the southern Yucatán: Has human activity resulted in more
1286 resilient forests? Forest Ecology and Management 310: 812–820.
1287
1288 Mikita, T., and M. Klimánek. 2010. Topographic exposure and its practical applications. Journal
1289 of Landscape Ecology 3: 42-51.
1290

Muchoney, D.M., S. Iremonger, and R. Wright. 1994. Rapid Ecological Assessment: Blue and John Crow Mountains National Park, Jamaica. The Nature Conservancy, Arlington Virginia, USA.

Negrón-Juárez, R., D. B. Baker, J. Q. Chambers, G. C. Hurtt, and S. Goosem. 2014a. Multi-scale sensitivity of Landsat and MODIS to forest disturbance associated with tropical cyclones. Remote Sensing of Environment 140: 679–689.

Negrón-Juárez, R. I., J. Q. Chambers, G. C. Hurtt, B. Annane, S. Cocke, M. Powell, M. Stott, S. Goosem, D. J. Metcalfe and S. S. Saatchi. 2014b. Remote sensing assessment of forest disturbance across complex mountainous terrain: The pattern and severity of impacts of tropical cyclone Yasi on Australian rainforests. Remote Sensing 6: 5633–5649.

Pettit, L. 1990. The conditional predictive ordinate for the Normal distribution. Journal of the Royal Statistical Society, Series B 56: 3–48.

Pike, R.J., I. Evans, and T. Hengl. 2008. Geomorphometry: A Brief Guide. In Hengl, T. and Reuter, H. I. (eds.), Geomorphometry - Concepts, Software, Applications. Series Developments in Soil Science, Volume 33, Elsevier, 3-33.

R Development Core Team. 2017. R: "A Language and Environment for Statistical Computing." R Foundation for Statistical Computing, Vienna. http://www.R-project.org/.

1314 Rossi, E., I. Granzow de la Cerda, C. D. Oliver, and D. Kulakowski. 2017. Wind effects and
1315 regeneration in broadleaf and pine stands after hurricane Felix (2007) in Northern
1316 Nicaragua. Forest Ecology and Management 400: 199–207.
1317
1318 Roxburgh, S. H., K. Shea, and J. B. Wilson. 2004. The intermediate disturbance hypothesis:
1319 patch dynamics and mechanisms of species coexistence. Ecology 85: 359–371.
1320
1321 Rue, H., and Martino, S. 2007. Approximate Bayesian inference for hierarchical Gaussian
1322 Markov random field models. Journal of Statistical Planning and Inference 137: 3177–3192.
1323
1324 Rue, H., S. Martino, and N. Chopin. 2009. Approximate Bayesian inference for latent Gaussian
1325 models using integrated nested Laplace approximations (with discussion). Journal of the Royal
1326 Statistical Society, Series B 71:319–392.
1327
1328 Rue, H., A. Riebler, S. H. Sørbye, J. B. Illian, D. P. Simpson, and F. K. Lindgren. 2017.
1329 Bayesian computing with INLA: a review. Annual Review of Statistics and its Application 4:
1330 395–421.
1331
1332 Ruel, J. C., S. J. Mitchell, and M. Dornier. 2002. A GIS based approach to map wind exposure
1333 for windthrow hazard rating. Northern Journal of Applied Forestry 19: 183–187.
1334

1335 Runkle, J. R., 1985: Disturbance regimes in temperate forests. In Pickett, S. T. A., and White, P.
1336 S. (eds.), The Ecology of Natural Disturbance and Patch Dynamics. New York: Academic Press,
1337 17–34.
1338
1339 Scatena, F. N., and M. C. Larsen. 1991. Physical aspects of Hurricane Hugo in Puerto Rico.
1340 Biotropica 23: 317–323.
1341
1342 Schielzeth, H., and S. Nakagawa. 2013. Nested by design: model fitting and interpretation in a
1343 mixed model era. Methods in Ecology and Evolution 4: 14–24.
1344
1345 Shea, K., Roxburgh, S. H., and Rauschert, E. S. 2004. Moving from pattern to process:
1346 coexistence mechanisms under intermediate disturbance regimes. Ecology Letters 7: 491–508.
1347
1348 Sheil, D. 1999. Tropical forest diversity, environmental change and species augmentation: after
1349 the intermediate disturbance hypothesis. Journal of Vegetation Science 10: 851–860.
1350
1351 Sheil, D., and D. F. Burslem. 2013. Defining and defending Connell's intermediate disturbance
1352 hypothesis: a response to Fox. Trends in ecology & evolution 28: 571–572.
1353
1354 Simpson, D., H. Rue, A. Riebler, T. G. Martins, and S. H. Sørbye. 2017. Penalising model
1355 component complexity: A principled, practical approach to constructing priors. Statistical
1356 Science 32: 1–28.
1357

1358 Spiegelhalter, D.J., N.J. Best, B.P. Carlin, and A. Van Der Linde. 2002. Bayesian measures of
1359 model complexity and fit. Journal of the Royal Statistical Society: Series B (Statistical
1360 Methodology) 64: 583–639.
1361
1362 Tanner, E.V.J. 1977. Four montane rain forests of Jamaica: a quantitative characterization of the
1363 floristics, the soils and the foliar mineral levels, and a discussion of the interrelations. Journal of
1364 Ecology 65: 883–918.
1365
1366 Tanner, E. V. J., and P. J. Bellingham 2006. Less diverse forest is more resistant to hurricane
1367 disturbance: evidence from montane rain forests in Jamaica. Journal of Ecology 94: 1003–1010.
1368
1369 Tanner, E. V., F. Rodriguez-Sanchez, J. R. Healey, R. J. Holdaway, and P. J. Bellingham. 2014.
1370 Long-term hurricane damage effects on tropical forest tree growth and mortality. Ecology 95:
1371 2974–2983.
1372
1373 Uriarte, M., J. Thompson, and J. K. Zimmerman. 2019. Hurricane María tripled stem breaks and
1374 doubled tree mortality relative to other major storms. Nature Communications 10: 1362.
1375
1376 Vandermeer, J., I. G. de la Cerda, D. Boucher, I. Perfecto, and J. Ruiz. 2000. Hurricane
1377 disturbance and tropical tree species diversity. Science 290: 788–791.
1378
1379 Weaver, P. L. 1986. Growth and age of *Cyrilla racemiflora* L. in montane forests of Puerto
1380 Rico. Interciencia 11: 221–228.

Weaver, P. L. 2002. A chronology of hurricane induced changes in Puerto Rico s lower montane rain forest. Interciencia 27: 252–258.

Webb, L. J. 1958. Cyclones as an ecological factor in tropical lowland rain-forest, north Queensland. Australian Journal of Botany 6: 220–228.

Xi, W., R. K. Peet, J. K. Decoster, and D. L. Urban. 2008. Tree damage risk factors associated with large, infrequent wind disturbances of Carolina forests. Forestry 81: 317–334.

Zheng, B. 2000. Summarizing the goodness of fit on generalized linear models for longitudinal data. Statistics in Medicine 19: 1265–1275.

Zimmerman, J. K., E. M. Everham III, R. B. Waide, D. J. Lodge, C. M. Taylor, and N. V. Brokaw. 1994. Responses of tree species to hurricane winds in subtropical wet forest in Puerto Rico: implications for tropical tree life histories. Journal of Ecology 82: 911–922.

Zuur, A. F., E N. Ieno, and A. A. Saveliev. 2017. Beginner's guide to spatial temporal and spatial-temporal ecological data analysis with R-INLA. Volume I: Using GLM and GLMM. Highland Statistics Ltd., Newburgh United Kingdom.

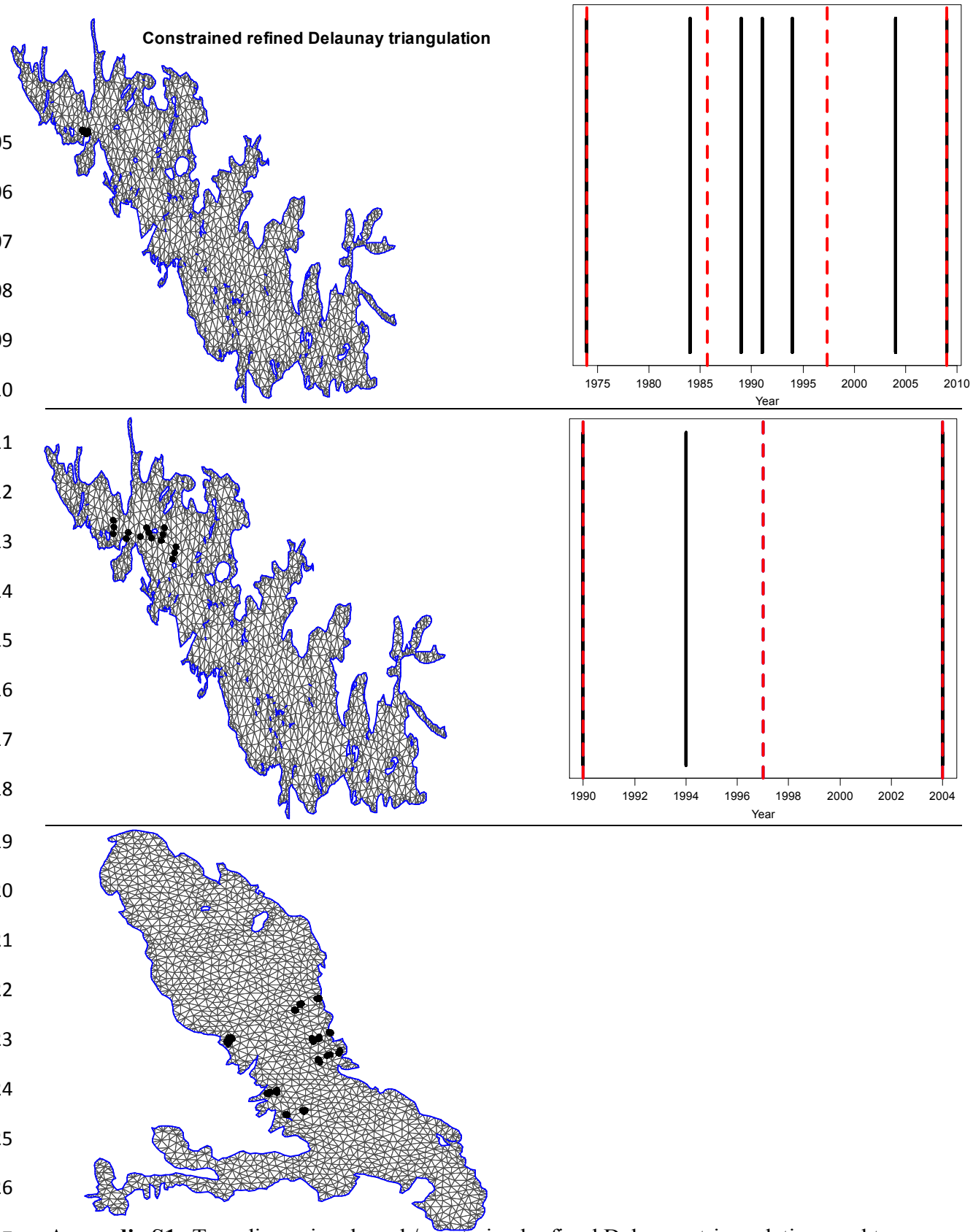

Appendix S1. Two-dimensional mesh/constrained refined Delaunay triangulation used to calculate the Gaussian (Markov) random field in the SPDE approach (left) and the knots (dashed red lines) used for a one-dimensional mesh for the temporal component of the models (right) for the Blue Mountains (top: Tanner's plots; middle: Bellingham's plots). The bottom mesh is for

1431 the John Crow Mountains (Luke et al.'s (2016)) plots. The plots are shown as black closed
1432 circles. The solid black lines are the censuses.